University of New Mexico

UNM Digital Repository

1-1-2022

Cancer Vaccines from Cryogenically Silicified Tumour Cells Functionalized with Pathogen-associated Molecular Patterns

Jimin Guo
Department of Internal Medicine, University of New Mexico Health Science Center, Albuquerque, NM, USA

Henning De May
Department of Obstetrics & Gynecology, University of New Mexico Health Science Center, Albuquerque, NM, USA

Stefan Franco
Department of Internal Medicine, University of New Mexico Health Science Center, Albuquerque, NM, USA

Achraf Noureddine
Department of Chemical and Biological Engineering, University of New Mexico, Albuquerque, NM, USA

Lien Tang
Department of Chemical and Biological Engineering, University of New Mexico, Albuquerque, NM, USA

See next page for additional authors

Recommended Citation

Guo J, De May H, Franco S, Noureddine A, Tang L, Brinker CJ, Kusewitt DF, Adams SF, Serda RE. Cancer vaccines from cryogenically silicified tumour cells functionalized with pathogen-associated molecular patterns. Nat Biomed Eng. 2022 Jan;6(1):19-31. doi: 10.1038/s41551-021-00795-w. Epub 2021 Nov 1. PMID: 34725505; PMCID: PMC8792180.

Authors

Jimin Guo, Henning De May, Stefan Franco, Achraf Noureddine, Lien Tang, C J. Brinker, Donna F. Kusewitt, Sarah F. Adams, and Rita E. Serda

Cancer vaccines from cryogenically silicified tumour cells functionalized with pathogen-associated molecular patterns

Jimin Guo[1,&], **Henning De May**[2,&], **Stefan Franco**[1], **Achraf Noureddine**[3], **Lien Tang**[3], **C.J. Brinker**[3], **Donna F. Kusewitt**[1], **Sarah F. Adams**[2,#], **Rita E. Serda**[1,#,*]

[1]Internal Medicine, University of New Mexico Health Science Center, Albuquerque, NM 87131, USA

[2]Department of Obstetrics & Gynecology, University of New Mexico Health Science Center, Albuquerque, NM 87131, USA

[3]Chemical and Biological Engineering, University of New Mexico Albuquerque, NM 87131, USA

Abstract

The production of personalized cancer vaccines made from autologous tumour cells involves complex and laborious processes. Here, we show that cancer vaccines can be made via the cryogenic silicification of tumour cells, which preserves tumour antigens within nanoscopic layers of silica, followed by the decoration of the silicified surface with pathogen-associated molecular patterns. These pathogen-mimicking cells activate dendritic cells, and enhance the internalization, processing and presentation of tumour antigens to T cells. In syngeneic mice with high-grade ovarian cancer, a cell-line-based silicified cancer vaccine supported the polarization of CD4$^+$ T cells toward the T-helper-1 phenotype in the tumour microenvironment, and induced tumour-antigen-specific T-cell immunity, resulting in complete tumour eradication and in long-term animal survival. In the setting of established disease and a suppressive tumour microenvironment, the vaccine synergized with cisplatin. Silicified and surface-modified cells from tumour samples are amenable to dehydration and room-temperature storage without loss of efficacy, and may be conducible to making individualized cancer vaccines across tumour types.

One-sentence editorial summary:

Efficacious cancer vaccines can be made via the cryogenic silicification of tumour cells followed by the decoration of the silicified surface with pathogen-associated molecular patterns.

Recent advances in strategies to engage the immune system for cancer therapy have established immunotherapy as an option for cancer treatment [1]. Evidence that cancer can elicit tumour-specific immune responses has additionally spurred the development

of therapeutic vaccines [2-4]; however the clinical efficacy of tumour vaccines is hindered by a lack of broadly expressed tumour antigens in many cancers. To circumvent this, autologous tumour cells have been used for the construction of polyclonal individualized tumour vaccines, addressing the lack of universally expressed tumour antigens and the risk of immune escape with treatments that target single antigens. Neoantigens can be highly immunogenic, however, immunosuppressive mechanisms that evolve during cancer progression dampen effective anti-tumour immune responses [5,6]. Efforts to overcome suppressive effects of the TME in designing cell based vaccines include *ex vivo* genetic modification of tumour cells, or electroporation/co-incubation of tumour cell lysate or personalized peptides with autologous dendritic cells (DC) [7-10], as well as the use of pathogens or pathogenic components as vaccine adjuvants [11,12]. Although these approaches show promise, clinical applications have been limited by lengthy and complex production requirements [6]. Here we demonstrate that advances in material science, specifically cell cryo-silicification, can be leveraged to overcome these hurdles to rapidly create stable biomineralized tumour cells that function as a modular vaccine for the development of a highly effective personalized immune therapy.

Various organisms, such as hot-spring bacteria [13] and unicellular diatoms [14], create amorphous silica exoskeletons from environmentally available soluble silica within acidified compartments that protect them from environmental stressors and mediate permeability and osmotic stress. In previous work, we demonstrated that immersion of fixed cells in acidified solutions of soluble silica preserved cellular features via a self-limiting biosilicification process wherein soluble silica was catalytically condensed to form nanoscopic amorphous silica coatings proximal to interfacial cationic proteins at all intracellular and extracellular biomolecular interfaces [15]. Here we improved the biosilicification process and adapted it for vaccine development through a cryo-silicification process that avoids aldehyde fixation to create a modular vaccine that preserves an individual patient's cancer neoantigens. Further, the thin, hydroxylated silicified cell surface enables modification with biofunctional moieties [here Toll-like receptor (TLR) ligands] to enhance cell immunogenicity and direct downstream immune responses for therapeutic benefit [16,17].

TLRs on the surface of DC recognize highly conserved pathogen-associated molecular patterns (PAMPs). For example, TLR4 recognizes lipopolysaccharide (LPS), or its derivative monophosphoryl lipid A (MPL), from gram-negative bacteria, whereas TLR9 recognizes bacterial hypomethylated CpG DNA motifs. We previously reported enhanced phagocytosis of microparticles by DC through MPL biniding to the microparticle surface. This was accompanied by increased DC expression of CD40, CD80, CD86, as well as MHC class I and II molecules [18]. This study examines the impact of coating silicified tumour cells with TLR ligands on DC functions, with an emphasis on internalization, antigen presentation, and therapeutic efficacy of the resulting bacterial mimic cancer vaccine. An advantage of attaching TLR ligands to the silicified cell surface is multivalent activation of surface and endosomal TLRs on antigen presenting cells (APC) [16,19,20]. In addition to enhancing endocytosis, TLR ligands affect phagosomal maturation governing proteolytic activity and peptide generation, as well as downstream effects such as fusion with the MHC class II compartment, expression of costimulatory molecules, and cytokine production driving T cell polarization [21] [22]. The combination of TLR4 and TLR9 agonists has been shown to polarize

macrophages, DC and natural killer cells towards a T helper (Th)1 phenotype [16], thereby directing and amplifying anti-tumour immune responses.

Here we demonstrate the therapeutic impact of a vaccine comprised of silicified cancer cells presenting TLR ligands in syngeneic ovarian cancer models. Using high grade serous syngeneic ovarian cancer mouse models, we demonstrate successful induction of protective tumour antigen-specific T cell immunity and complete elimination of established tumours in vaccinated mice. While these experiments demonstrate the efficacy of silicified cell vaccines in ovarian cancer, this modular approach to cancer vaccine development can be adapted broadly for other tumour types.

RESULTS

Tumour cell silicification establishes a modular approach for vaccine development

Ex vivo silicification of cancer cells as a method of fixation enables preservation of cell integrity and the biofunctionality of proteinaceous components, and enables surface functionalization with PAMPs (Fig. 1a). Importantly, this process represents a significant advance over prior work on cellular silicification [15] by eliminating aldehyde fixation, empowering improved biofunctionality of cellular components and removing the use of this cytotoxic material as a means of cell preservation. Cryo-silicification is technically simple and can be extended to any arbitrary cell type enabling personalization. In our standard procedure, cancer cells at a density of 3×10^6 cells/mL are suspended in a hypotonic aqueous solution of 100 mM NaCl and 10 mM TMOS at pH 3.0 for 10 minutes and then maintained for 24 hours at −80°C. With the goals of preserving cell integrity, limiting silica layer thickness, and avoiding cell aggregation, NaCl and TMOS concentrations were optimized (Supplemental Fig. 1-2). Scanning electron microscopy (SEM) and energy dispersive spectroscopy (EDS) analysis of silicified murine ovarian cancer cells confirmed the presence of organic matter (C and O) and elemental Si (Fig. 1b). Inductively coupled plasma-optical emission spectroscopy (ICP-OES) analysis of silicified cells demonstrated that this approach resulted in significantly lower Si content compared to silicification under higher silicic acid concentrations or temperature (Fig. 1c). Specifically, the overall extent of Si deposition/thickness was reduced 55-fold compared to published processes used for cell silicification [15]. This is important as it allows rapid silica dissolution (Fig. 1c), enabling the biomolecular functionality of the cellular components.

For these experiments, we employed high grade syngeneic ovarian cancer models. The BR5-Akt cell line, kindly provided by Sandra Orsulic, was used for the majority of experiments because this model was developed on an FVB background, facilitating *in vivo* imaging with the IVIS Spectrum. An ID8ova cell line, developed from the ID8 cancer model established in a C57BL/6 strain and transduced to express the model antigen ovalbumin was used for *in vitro* assessments of tumour antigen-specificity.

Surface modification of silicified (Si)-cells to enable functionalization

The innovation of this approach to tumour cell fixation for vaccine development is based on the properties of silica that enable surface binding of adjuvants or other immunomodulatory

compounds. The native chemistry of the silicified cell surface is dominated by hydroxyl (silanol Si-OH) groups. At physiological pH, the silanol groups are largely dehydroxylated creating an anionic (Si-O⁻) surface that adsorbs cationic molecules and polymers that in turn can adsorb and retain anionic ligands. Adsorption of polyethyleneimine (PEI), polylysine (PL) or chitosan (Chit) on the silicified (Si) cell surface each reversed the negative Si-cell surface/zeta potential (Fig. 2d; Supplemental Fig. 3a). Further, based on zeta potential analysis, PEI, unlike the other cationic molecules, facilitated homogeneous MPL binding to the silicified cell surface (Supplemental Fig. 3b), and optimal activation of DC based on CD40 surface expression (Supplemental Fig. 3c). PEI, an organic cationic polymer that has been reported to be a TLR4 or TLR5 ligand with the ability to increase the immunogenicity of DNA-based vaccines and nanoparticles [23-25], displayed higher binding to Si-cells compared to aldehyde-fixed cells using zeta potential as a metric for cell modification (Supplemental Fig. 3d). Based on these cumulative properties, PEI was selected for vaccine development. We next selected two TLR agonists for silicified cell surface modification and optimized binding capacity (Supplemental Fig. 4). Due to the reported synergistic activity and Th1 skewing by CpG and MPL in cancer models [25,26], we compared single and dual agonist effects using our BR5-Akt mouse model. Vaccination with Si-PEI-CpG-MPL BR5-Akt (hereafter Si vaccine) cells resulted in optimal treatment outcomes (Extended Data Fig. 1). A vaccine dose of 3×10^6 cells (optimized herein) contains approximately 5 μg CpG, 4 μg MPL, 54 μg PEI and 0.2 μg Si, with a mass ratio of 1000:0.06:18:1.7:1.4 for cells:Si:PEI:CpG:MPL (assuming a mass of 1 mg for 1×10^6; Fig 1e).

Silicified cells are safe for use in vivo

To evaluate the safety of Si vaccine cells for cancer treatment, we assessed their viability *in vitro* and *in vivo*. During vaccine preparation, cancer cells are exposed to an acidic, hypotonic silicic acid solution, followed by freezing at −80°C, and surface modification. Using an absence of ATP production as an *in vitro* measure of metabolic activity, these processing methods resulted in complete cell death (Fig. 1f). Silicifed cells were then incubated in 0.2 mg/ml PEI for 10 minutes. PEI is a cationic macromolecule, and both branched and linear free PEI can compromise membrane integrity and initiate cell apoptosis [27]. We have reported that while small nanoparticles can be cytotoxic *in vitro* under typical cell culture conditions, larger entities coated with PEI do not induce toxicity [28]. In addition, in the presence of physiologically relevant levels of serum, the cationic surface charge of PEI-coated particles is masked with serum proteins, mitigating the biological impact. As an additional assessment for viability, cellular uptake of propidium iodide (PI) was evaluated by flow cytometry. Notably, scatter dotplots of live or Si tumour cells supported retention of cell structure following silicification, as expected. In these experiments, all silicified cells displayed intracellular PI staining (Fig. 1g), confirming that silicified cells are not viable. Finally, to ensure that these cells could not establish tumours *in vivo,* luciferase positive silicified cells were injected intraperitoneally into mice and tumour growth was assessed for 25 days. None of these mice developed any bioluminescent evidence of tumour viability (Fig. 1h). Additionally, mice injected with Si vaccine cells by subcutanesous administration lacked evidence of any tumour at the injection site by histologic assessment (Supplemental Fig. 5). With confirmation that silicified tumour cells can be safely administered *in vivo*, we proceeded with further vaccine optimization.

Surface modification of Si-cells with TLR agonists enhances DC uptake and activation

Engagement of TLR4 and TLR9 on antigen-presenting cells (APC) has been shown to promote antigen internalization, cytokine secretion, and expression of costimulatory molecules and major histocompatibility complex (MHC) [16]. To test whether surface modification with CpG and MPL promoted Si vaccine cell uptake and processing by APC, we performed co-culture experiments with bone marrow-derived DC *ex vivo.* Confocal microscopy and flow cytometry confirmed that Si vaccine cells are engulfed by DC *in vitro* within one hour (Fig. 2a-d; Extended Data Fig. 1a). To specifically track Si vaccine cells (blue: actin; green: tubulin; violet: DAPI), they were loaded with fluorescent nanoparticles (red; rhodamine B) prior to silicification (Fig. 2a). The actin fluorescence is shown with variable thresholding in Figures 2a (blue) and 2b (red) to enable identification of intracellular and surface bound modified Si tumour cells. Internalization of Si-PEI-CpG-MPL, Si-PEI, or Si-only tumour cells by DC was compared to that of live or paraformaldehyde-fixed tumour cells using flow cytometry and Cell Trace Far Red-labeled cells. Silicified tumour cells bound with CpG and MPL had a 9-fold increase in uptake compared to live or fixed tumour cells (Fig. 2c). The increase in uptake of Si vaccine cells is based on the ability of TLR ligands to specifically promote phagocytosis in both murine and human cells through induction of a phagocytic gene program, with TLR9 being the strongest promoter [29]. Activation of TLRs was also supported by an increase in CD80 expression by DC (Extended Data Fig. 2b).

To confirm DC internalization of intact cancer cells, the Amnis Imagestream was used to image and quantitate vaccine uptake. After 24 hours, 64% of Si vaccine cells were internalized by BMDC in vitro (Fig. 2d). In tumour-bearing mice, the majority of Si vaccine cells administered IP localized to filtering (spleen and liver) and lymphatic tissues (Extended Data Fig. 2c). The majority of vaccine, which was both free and cell-internalized, was located in CD11c rich regions (milky spots) of the omentum (Extended Data Fig. 2d).

Finally, to assess tumour-specific antigen presentation in the context of MHC I, we used the ID8ova cell line that expresses the model antigen ovalbumin. Ova peptide (SIINFEKL) presentation on MHC I by DC was assessed by flow cytometry analysis after 72 hour co-culture with Si ID8ova vaccine cells. This time point was selected based on previous work demonstrating optimal target antigen presentation with mesoporous silicon microparticles [16]. These experiments demonstrated that DC processing of a model antigen and peptide presentation was superior using Si vaccine cells compared to irradiated cancer cells (Fig. 2e).

Silicified, surface modified tumour cells generate tumour-specific immunity in vivo

To evaluate the immunogenicity of Si vaccine cells *in vivo*, albino C57BL/6 mice were injected with Si ID8ova vaccine cells. Three weeks later, mice were challenged IP with live tumour cells. Tumour burden was monitored based on bioluminescence with IVIS Spectrum imaging and quantified as photons/second (p/s; Fig. 3a). Si vaccine cell treated mice displayed complete blockade of tumour engraftment in contrast to sham PBS (no Tx) or Si tumour cell treated mice, which demonstrated partial resistance to tumour growth (n=10/group). To obtain a quantitative measure of cellular immune response, the enzyme-

linked immunospot (ELISPOT) was used to detect IFNγ production at the single cell level as an indicator of antigen specific T cell number [30]. Peritoneal immune cells from C57BL/6 mice vaccinated with Si ID8ova vaccine cells were stimulated with ovalbumin for 19 hours, and IFNγ colometric spots were counted. There was a 4.6-fold increase in IFNγ-producing T cells from vaccinated mice compared to sham PBS treated mice (Fig 3b).

A similar survival benefit was seen using the BR5-Akt tumour model. Notably, in these experiments, antigen specificity was confirmed using vaccination with TLR agonist-coated mesoporous silica nanoparticles (MSN) or silicified leukocytes as controls. Additonal controls were sham PBS, Si tumour cells, or oxidized tumour cell lysate, the latter including TLR agonists. All injections were IP (single dose on Day −21, with the addition of SC administration of 1 verses 2 doses of vaccine. Tumour cell bioluminescence supported complete blockade of tumour engraftment in all IP and SC vaccinated mice (Fig. 3c) In contrast, TLR agonist coated MSN or Si leukocyte treated mice showed progressive tumour growth requiring euthanization by Day 30, confirming that tumour cell, and presumable tumour antigens, are required for immune protection. Also, tumour cell lysate combined with TLR ligand was insufficient to protect mice, supporting that the intact tumour cell with TLR agonist is needed.

Therapeutic vaccination in vivo results in durable survival benefit

The ability of vaccination to clear pre-existing tumours was evaluated in FVB mice with BR5-Akt-Luc2 tumours. First, an optimal route of administration, dose and schedule, were established to optimize tumour clearance and survival (Extended Data Fig. 3, Supplemental Fig. 6) Subsequently, this optimal protocol using Si vaccine cells was directly compared with an irradiated tumour cell vaccine that has been advanced to clinical trials [31]. Results from these studies demonstrated that Si vaccine cells completely eliminate existing peritoneal tumours with clear superiority over the irradiated tumour cell vaccine (Fig. 4a-b). Modification of irradiated cells with PEI, CpG and MPL improved performance, but even with these changes, the irradiated tumour cell vaccine was inferior to Si vaccine cells.

Vaccine can be dehydrated without loss of efficacy

In these comparisons, additional advantages of cell silicification were identified. Specifically, silicification enables cancer cells to be dehydrated and stored at room temperature (Fig. 4c). Following rehydration, the Si cells can be coated with TLR ligands or other immune agonists. Notably, the therapeutic efficacy of vaccination was not diminished in mice injected with rehydrated Si vaccine cells that had been stored at room temperature for two weeks compared with mice vaccinated with fresh modified Si vaccine cells (Fig. 4d). In contrast, irradiated cell vaccines did not survive dehydration, remaining aggregated after attempts at rehydration. The ability to store cellular tumour vaccines at room temperature is a significant advance that is expected to facilitate production and expand access to personalized cancer immune therapy.

Vaccination promotes effector function of tumour-associated lymphocytes

Vaccinated mice had a significant increase in the total number of CD4^{+} and CD8^{+} T cells and a marked increase in the proportion of effector memory cells in the peritoneal tumour

environment (Fig. 5a, Extended Data Fig 4, Supplemental Fig. 7-8). Notably, Si tumour cell vaccination reduced the mean CD4/CD8 ratio from 6.0 to 1.5 (Fig. 5b, ranges 4.5-8.7 and 1.1-1.9 for no Tx and vaccinated groups), which is associated with improved outcomes in patients with ovarian cancer [32]. In addition, vaccination significantly increased Th1 polarization among CD4+ T cells while reducing the percentage of suppressive regulatory CD4+ T cells (Fig. 5c). Increased levels of IL-2, IFNγ, and TNFα production by both CD4+ and CD8+ T cells was observed following *ex vivo* stimulation (Fig. 5c; Supplemental Fig. 9). Ascites fluid TNFα was also elevated following vaccination (Fig. 5d).

To assess for the induction of adaptive immunity in response to vaccination, the cytotoxic capacity of peritoneal CD8+ T cells isolated from vaccinated mice were tested *ex vivo.* These experiments demonstrated enhanced cancer cell killing compared with CD8+ T cells from naïve mice (Fig. 5e). The successful induction of an anti-tumour T cell response *in vivo* following vaccination was evaluated with adoptive transfer experiments. 2x10^5 magnetically enriched peritoneal CD8+ cells collected from vaccinated tumour-bearing mice were transferred to tumour-naïve mice 24 hours prior to tumour challenge. CD8+ cells from unvaccinated, tumour-naive) mice were used as a negative control. Results from these experiments demonstrated that tumour-associated CD8+ T cells from vaccinated mice successfully protected recipients from tumour challenge, while adoptively transferred T cells from naïve mice did not (Fig. 5f). Collectively, these results demonstrate that vaccination with Si modified cells elicits a tumour-specific T cell response and protective immune memory.

Vaccination synergizes with platinum chemotherapy to clear established tumour

In our initial experiments we treated mice at a time point at which they had small volume disseminated tumour. This mimics the treatment of patients after cytoreductive surgery, which is a central component of ovarian cancer treatment. Because treatment of both primary and recurrent ovarian cancer also includes platinum-based chemotherapy, we tested whether Si tumour cell vaccine could synergize with cisplatin to enhance tumour clearance in the setting of bulky disease. In these experiments, treatment with cisplatin was delayed until day 9 after tumour challenge. Mice received 2 mg/kg cisplatin IP [33], followed by Si vaccine cells on days 10 and 17. Tumour burden was measured by bioluminescence. Results from these experiments demonstrated evidence of therapeutic synergy with improved survival in the combination treatment group compared with either cisplatin or vaccination alone (Fig. 6a-b). As seen with early time point therapy, the proportion of functionally activated T cells expressing IFNγ and TNFα was elevated in vaccinated mice, with cisplatin also stimulating production of TNFα (Fig. 6b).

Ascites can be used for Si tumour cell vaccine development

Translating our findings to develop Si vaccines for cancer patients will require a source of autologous tumour cells. Clinically, ovarian cancer presents at late stages of disease when patients have metastases throughout the peritoneal cavity and accumulation of malignant ascites. To test whether tumour cells from ascites could be used for vaccine development, we collected ascites samples from mice with late-stage BR5-Akt tumours (Fig. 7a; Supplemental Fig. 9a-b). Tumour cells from ascites were enriched by filtration capture

and silicified using the protocol developed using cancer cell lines (Fig. 7b). Vaccination using silicified mouse ascites tumour cells at the same dose and schedule optimized previously demonstrated equivalent efficacy as vaccination using Si vaccine cells grown *in vitro* (Fig. 7c). Secondary tumour challenge on Day 36 was rapidly cleared (Fig. 7d). These results indicate that vaccine production is feasible using available tumour samples to create personalized vaccines.

To demonstrate vaccine production from cancer patients, ascites cancer cells were enriched by filtration capture (Fig. 7e), silicified and coated with TLR ligands using PEI, MPL, and human specific CpG 2006 (7909). Ascites CD11c$^+$ DC, enriched by loose attachment to plastic tissue culture dishes, internalized 96% of Si vaccine cells within 24 hours (Fig. 7f). Vaccine treated DC displayed elevated CD86 expression within the same time frame (Fig. 7g). These results support that vaccination production is feasible from human ascites samples.

Vaccination with silicified tumour cells is not associated with significant immune-related toxicity

In preparation for clinical translation, we evaluated mice for any evidence of toxicity following vaccination. Histopathologic analysis performed by a board-certified veterinary pathologist showed pronounced necrosis in small residual islands of tumour in vaccinated mice associated with marked immune cell infiltration (Supplemental Fig. 10). Increased numbers of leukocytes were noted in peritoneal samples from vaccinated mice but no evidence of suppurative peritonitis was found. No significant differences in complete blood count or electrolyte levels were observed in vaccine recipients compared with untreated controls (Extended Data Fig. 5a, Supplemental Fig. 11). Consistent with a T cell mediated immune response, treatment of tumour-bearing mice with Si vaccine cells significantly increased blood lymphocytes (Extended Data Fig. 5b). Vaccination had no impact on renal or hepatic function (Extended Data Fig. 5c,d) and no vaccinated mice developed rash, alopecia, diarrhea or weight loss suggestive of treatment toxicity.

Discussion

Herein we describe a modular vaccine for personalized immune therapy that demonstrates durable therapeutic efficacy in high-grade serous ovarian cancer models. This strategy introduces substantial advantages over existing cell-based vaccines, including preserved tumour antigens, the opportunity for long-term dry-storage, surface binding capacity for multivalent presentation of immune modulators, activation of both innate and adaptive immunity, potent therapeutic efficacy without demonstrated toxicity, and simplified production and storage requirements for broader accessibility.

Cell silicification enables the ability to engineer cells to safely deliver target antigens and immune modulators. Because the silica surface is highly absorbent and readily binds adjuvants such as CpG and MPL, these cells acquire surface functionalization that can be exploited to direct specific immune responses. Coating silicified cancer cells with TLR agonists successfully induced innate and cellular immune activation, demonstrating enhanced internalization and processing by DC. Notably, DCs possess a unique mechanism

for phagosome maturation, maintaining the phagosome at an alkaline pH of 7 to 7.5 in the first few hours after phagocytosis [34]. During this time, DCs recruit NOX2 leading to proton consumption by oxygen radicals and cell neutralization to facilitate peptide loading onto MHC molecules [35]. These same conditions also favor siloxane bond (Si-O-Si) hydrolysis, facilitating silica dissolution [36]. Adsorption of PEI to silica further promotes silica dissolution at neutral and acidic pH due to pH buffering [37]. Our data demonstrate that DC activation in response to the vaccine is associated with the induction of tumour-specific adaptive immunity and protection against secondary tumour challenge. While these proof-of-principle experiments used TLR ligands as bound adjuvants for vaccine development, the silicified cell surface can bind a broad array of molecules, presenting diverse opportunities for immune modulation and targeted therapy. Notably, the Si vaccine can be dehydrated and stored at room temperature. Upon rehydration, the choice of surface-bound adjuvant could be based on an individual patient's response to treatment or tailored for the immune landscape of a patient's tumour. In addition, the integration of antibodies or molecules that reverse inhibitory pathways in the tumour microenvironment would be expected to sustain the activation of cancer-specific T cells generated in response to the vaccine.

Importantly, women with ovarian cancer typically present with widely metastatic disease, often associated with abdominal ascites. Ascites fluid can be removed percutaneously with paracentesis or evacuated at the time of tumour debulking surgery. We have demonstrated that ascites samples can be used to develop a highly effective silicified vaccine, presenting a clinically feasible strategy for rapid vaccine development. This treatment paradigm presents an optimal opportunity for vaccination after surgical cytoreduction and frontline chemotherapy, when tumour burden is low. It is notable, however, that vaccination also enhances survival in the setting of bulky disease in combination with platinum agent, cisplatin, which is considered the backbone of treatment for ovarian cancer, including recurrent disease. These results demonstrate that vaccination can be effectively integrated into the established treatment protocols for this disease to enhance patient outcomes.

Prior approaches to creating personalized vaccines that have been tested in the clinic include DC vaccines based on ex vivo differentiation of peripheral blood monocytes, followed by pulsing with oxidized tumour cell lysate [7,38]. Also, co-delivery of irradiated cells with BCG [39] or nanoparticles (e.g. Cowpea Mosaic Virus [40]), or nanoparticles loaded with oxidized tumour cell lysate [41]. These processes can be laborious and costly [7,42,43], or may rely on synthetic or heterogenous materials. In addition to low cost and rapid production (within 24 hours), an additional benefit of the silicified cancer cell approach is the combination of tumour antigens and TLR ligands in a single construct. Nair-Gupta et al. [44] demonstrated that TLR-loaded endosomes fuse with Rab11a positive MHCI storage vesicles in DC, enhancing cross presentation of antigens within the TLR-ligand containing endosomes. In summary, in addition to the Si vaccine out-performing and demonstrating markedly improved survival compared to a clinically-tested irradiated tumour cell vaccine, the ability to dehydrate the vaccine has the potential to address a global need for versatile tumour vaccines with the potential to reduce existing disparities in access to cancer immune therapy. As a result, this technology would transform both the production and distribution of cancer vaccines and facilitate the integration of immune therapy into cancer treatment protocols.

Outlook

In summary, we have introduced a highly effective autologous cancer vaccine. The modular approach enables vaccine loading with unique molecules, either within or on the silicified cell surface, to drive diverse responses, potentially across multiple tumour types. Vaccine delivery directly to the tumour microenvironment reprograms the suppressive milieu, supporting the development of anti-tumour immune responses and immunological memory. In addition, our approach simplifies vaccine production and distribution, facilitating the integration of immune therapy into current treatment protocols to improve survival outcomes.

Methods

Materials

Lipid A, monophosphoryl from Salmonella enterica serotype, tetramethyl orthosilicate, hydrochloric acid solution, sodium chloride, low molecular weight chitosan, poly-L-lysine, puromycin dihydrochloride, rhodamine B isothiocyanate mixed isomers, and 10% buffered formalin, were purchased from Sigma-Aldrich (St. Louis, MO, USA). CpG Oligonucleotide 1826 was purchased from Invivogen (San Diego, CA, USA), and polyethylenimine (25k linear) was purchased from Polysciences (Warrington, PA, US). Prolong™ Gold Antifade Mountant with DAPI, Alexa Fluor® 488 alpha tubulin antibody phosphate-buffered saline (PBS) and RPMI 1640 were purchased from Thermo Fisher Scientific (Waltham, MA, USA). Fetal bovine serum (FBS) was purchased from ATCC (Manassas, VA, USA). 0.05% EDTA trypsin solution, penicillin-streptomycin, and rhodamine or Alexa Fluor® 647 phalloidin were purchased from Life Technologies Corporation (Carlsbad, CA, USA). Dulbecco's Modified Eagle's Medium (DMEM) was obtained from Caisson Labs (Smithfield, UT, USA). Cell Titer-Glo 2.0 Assay was purchased from Promega (Madison, WI, USA). Recombinant murine granulocyte macrophage colony stimulating factor (GM-CSF) was purchased from R&D Systems (Minneapolis, MN, USA). XenoLight D-Luciferin Potassium Salt was purchased from Perkin Elmer (Boston, MA, USA). Reversible Strainers (37 μm mesh) were purchased from STEMCELL Technologies (Cambridge, MA, USA).

Antibodies

CD11c FITC (HL3*)*, CD11c FITC (B-ly6), CD326 (EpCAM, G8.8) APC, CD326 (MαH EpCAM IB7) eFluor 660, CD3 (17A2) APC-eFluor 780, CD4 (GK1.5) APC, CD8a (53-6.7) eFluor 450 and Alexa Flour 488, CD11b (M1/70) APC and FITC, CD11c (N418) PerCP-Cyanine5.5 and PECy7, CD40 (3/23) PE, CD44 (IM7) PerCP-Cyanine5.5, CD62L (L-selectin, MEL 14) FITC, CD152 (CTLA-4, UC10-4B9) PE and PerCp-Cy5.5, CD279 (PD-1, J43) PE-Cyanine7, FOXP3 (FJK-16s) PE, IFN gamma (XMG1.2) Alexa Fluor 488, MHC Class II (I A/I E) (M5/114.15.2) FITC, GATA-3 PerCP-eFlour 710 (TWAJ), TNFα PerCP-eFlour 710 (MP6-XT22), CD45R (B220) FITC, Fc receptor blockers (anti-CD16/CD32 (clone 2.4G2)), mouse IgG (31205), and LIVE/DEAD™ Fixable Aqua Dead Cell Stain Kit for 405 nm excitation were purchased from eBioscience™/Thermo Fisher Scientific. IL-4 – APC (11B11), CD152 (CTLA-4) PerCP, TIM3 (B8.2C12) APC and CD11c FITC (N418; Amnis BMDC and mouse tissues) were purchased from BioLegend. IL-2 PE (JES6-5H4) was purchased from BD Bioscience.

Cell lines and mouse models of ovarian cancer

The BRCA1-deficient BR5-Akt cell line, generated on an FVB background, was a kind gift from Dr. Sandra Orsulic (Cedars-Sinai) [45]. The ID8ova cell line, generated from C57BL/6 ovarian epithelial cells, and transfected to express ovalbumin constitutively, was a gift from Dr. George Coukos at the University of Pennsylvania [46]. Both ID8ova and BR5-Akt cell lines are syngeneic models of high-grade serous epithelial ovarian cancer. To monitor tumour burden using a bioluminescent tag, the cell lines were lentivirus transduced to constitutively express firefly2 luciferase. Cell lines were cultured in DMEM containing 10% FBS and 100 units/100 μg penicillin/streptomycin at 37°C and 5% CO_2. Trypsin-EDTA was used to harvest cells.

To prepare bone marrow-derived dendritic cells (DC), bone marrow was harvested from the femurs of female murine C57BL/6 or FVB mice using a 27 g needle and syringe to flush the marrow from the bone. RBC were lysed with BD Lysis buffer as described by the vendor. Cells were cultured in 6 well plates (3 ml/well) for 8-10 days in RPMI 1640 medium supplemented with 10% FBS, 100 mM β-mercaptoethanol, penicillin/streptomycin, and 10 ng/mL recombinant murine GM-CSF. Half of the media was replaced every 2-3 days with fresh media and cytokines. Human DCs were enriched from ascites samples by loose adhesion to plastic cell culture dishes.

Mice were purchased from Charles River or Jackson Laboratories and housed in a specific pathogen-free facility. All animal protocols were approved by the Institutional Animal Care and Use Committee (IACUC) at the University of New Mexico (Albuquerque, NM, USA). To generate consistent engraftment and predictable disease progression, 2×10^5 BR5-Akt-Luc2 or 1-5 x 10^6 ID8ova-Luc2 cells in 200 μL PBS were administered by intraperitoneal (IP) injection in 6-7 week old FVB or albino C57BL/6 female mice [47]. Mice were sacrificed when moribund or when weight reached 30 g due to ascites accumulation. Mice were monitored and weighed every 2-3 days. For studies that included subcutaneous (SC) tumours, female mice were injected with 200 μl PBS containing 2×10^5 BR5-Akt-Luc2 cells on the dorsal surface using isoflurane as an inhalation anesthetic.

Cell silicification

3×10^6 BR5-Akt or ID8ova cells, as well as leukocytes obtained from RBC lysed FVB mouse spleen, or human ascites cancer cells enriched by filtration capture, were washed with PBS, followed by physiological saline (154 mM NaCl), and then suspended in 1 mL silicic acid solution containing 10 mM TMOS, 100 mM NaCl and 1.0 mM HCl (pH 3.0), with scale up as needed. Optimization of conditions for biological use evaluated cell stability and dispersion following silicification in 5-100 mM TMOS, and 100 verses 154 mM NaCl. Following a 5-10 minute incubation at room temperature, the cell suspension was transferred to −80°C for 24 hours. Silicified cells were then washed with endotoxin-free water, followed by PBS. To compare Si content with published cell silicification techniques, cells were also silicified at room temperature in silicic acid solution containing 100 mM TMOS, 154 mM NaCl and 1.0 mM HCl (pH 3.0) for 24 hours [15].

Coating silicified cells with cationic polymer

Silicified cells were made cationic using chitosan, poly-L-lysine or PEI. 3×10^6 silicified cells were washed with water, followed by PBS, and then suspended in 1mL of 0.2 mg/mL PEI, 2 mg/mL chitosan, or 1 mg/mL poly-L-lysine in PBS. Following 10 minutes (or as indicated) of rotation at room temperature, cells were washed twice with PBS and zeta potentials evaluated.

Fluorescent PEI synthesis

PEI (5 g, 0.2 mmol) was dissolved in 5 mL ethanol and Cy3-NHS (10 mg/mL in DMF, 150 μL, 2 μmol) were added. The solution was rotated at 40 °C for 4 days. The mixture was concentrated using a rotavap, then 50 μL DMF were added to dissolve any unreacted dye. The mixture was centrifuged at 21,000g for 20 minutes and the isolated pellet was dissolved in ethanol and transferred to the rotavapor to remove DMF traces. After one hour, the PEI-Cy3 were dissolved in PBS at 0.5 mg/mL.

Adsorption of TLR ligand to silicified (Si) or irradiated cells

Silicified cells (12×10^6), with or without polymer coating, were washed with PBS and then suspended in 25 μL of 1 mg/mL MPL in DMSO. After 10 minutes incubation at room temperature, Si-PEI-MPL or Si-MPL cells (or their chitosan counterparts) were washed with PBS by centrifugation at 2000g for 5 minutes followed by suspension in PBS. 1826 oligodeoxynucleotide adsorption followed a similar protocol using 20 μL of 2 mg/mL CpG in endotoxin-free water for every 12×10^6 silicified cells. For dual adsorption of MPL and CpG, CpG was introduced first for 10 minutes, followed by the addition of MPL for an additional 10 minutes. To quantitate ligand loading, unbound fluorescent TLR ligand was measured using a BioTek microplate reader with excitation/emission at 470/560 nm for PEI-Cy3, and excitation/emission at 488/528 nm for CpG-FITC detection. MPL was quantified by absorption at 290 nm using a ThermoScientific NanoDrop 2000. Irradiated BR5-Akt cells were incubated with PEI, CpG and MPL using the same conditions optimized for silicified cells.

Dehydration and rehydration of vaccine cells

Silicified or irradiated cells (with or without PEI) were rinsed with PBS and then dried under vacuum at room temperature for 16h. Samples were stored at room temperature for 14 days. Prior to use, cells were rehydrated in PBS with vortexing and coated with PEI, CpG and MPL.

Zeta potential measurements

Zeta potential measurements were performed using the Malvern Zetasizer Nano-ZS (Westborough, MA, USA) equipped with a He–Ne laser (633 nm) and non-invasive backscatter optics (NIBS). Cells were suspended in 5 mM NaCl solution with measurements performed using the monomodal analysis tool. All reported values correspond to the average of at least three independent samples.

Optical Microscopy

For bright field imaging, cells were suspended in the water or PBS and imaged using the Nikon eclipse TS 100 inverted microscope equipped with a Nikon digital-sight DS-L3 camera.

In vitro DC internalization of fluorescent silicified cells

To image DC association with silicified cells, BR5-Akt cancer cells were first incubated with fluorescent lipid-coated mesoporous silica nanoparticles labeled with Cy3 or DyLight 488 and presenting MPL for 4-24 hours. Tumour cells were then silicified using optimized conditions and surface-masked with TLR ligands (as indicated). DC were seeded onto glass coverslips in 6-well plates at a density of 5×10^5 cells per well and the next day, fluorescent silicified vaccine cells were added and DC were incubated as indicated. DC were then washed with PBS and fixed with 4% paraformaldehyde for 15 minutes at room temperature followed by overnight incubation at 4°C. The following day, cells were washed with PBS, permeabilized with 0.1% Triton-X in PBS for 15 minutes, blocked with 1% BSA for 20 minutes, and then labeled with Alexa Fluor 647 phalloidin and in 1% BSA for 1 hour. After a final wash in PBS, coverslips were mounted on slides using Prolong Gold with DAPI. Images were acquired using a 63X/1.4NA oil objective in sequential scanning mode using a Leica TCS SP8 confocal microscope.

DC uptake of silicified cells was quantified using an Attune NxT Flow Cytometer (Thermo Fisher Scientific) or the Amnis ImageStream. Human ascites cancer cells or mouse BR5-Akt cells were stained with Cell Trace™ Far Red (CTFR; Thermo Fisher; 1:4000) prior to silicification. Silicified cells, surface modified with TLR ligands as indicated, were co-cultured with Cell Trace™ Violet (ThermoFisher; flow cytometry) or anti-CD11c FITC (Amnis; 1:1000) labeled human or mouse DCs for 1-24 hours as indicated at a ratio of 5:1 (vaccine:BMDC), and then analyzed by flow cytometry for double-positive cell populations or using the Amnis Imagestream. For Amnis analysis, a single cell population was gated on using a dot plot created using a bright-field laser (aspect ratio vs area), then focused bright-field cells were gated using a histogram of normalized frequency vs gradient RMS. Lastly, a dot plot was created showing internalized and non-internalized cells (intensity of CTFR channel vs intensity of FITC channel).

T cell killing assay

BR5-Akt cells were seeded into a 96 well plate at 1×10^3 cells per well in 200 μl followed by overnight incubation at 37°C in 5% CO_2. Peritoneal T-cells were purified using the Miltenyi Biotec $CD8a^+$ T cell Isolation Kit from vaccinated (day 57)/tumour-challenged or naive FVB mice. T-cells were added to cancer cells at a ratio of 5:1 and the cell impermeant nuclear dye YOYO™-3 iodide (1 mM in DMSO) was added at a dilution of 1:4000. Cells were put in the IncuCyte Live Cell Imaging System (Sigma Aldrich) and imaged for 48 hours with images acquired every 2 hours.

Interferon gamma (IFNγ) ELISpot

FVB mice were treated with PBS, Si-cells or vaccine on day 0 and peritoneal cells were isolated on day 14 as previously described. The ELISpot assay was performed as described

by the vendor (R&D Systems), with 2 x 10^5 RBC lysed peritoneal cells included per well/100 μl complete media. Ovalbumin was added at 15 μg/well for 19 hours at 37°C. Spots were counted manually using a dissection microscope.

Scanning electron microscopy (SEM) and energy dispersive X-ray (EDX) analysis

Silicified tumour cells were suspended in 100% ethanol and then dropped onto 5×5 mm glass slides. The glass slides were then mounted on SEM stubs using conductive adhesive tape (12 mm OD PELCO Tabs). SEM and EDX images were acquired under high vacuum at 7.5k using a FEI Quanta 3D Dualbeam FIB-FEGSEM with EDAX SDD EDS detector (Thermo Fisher Scientific, MA, USA).

Inductively Coupled Plasma-Optical Emission Spectroscopy (ICP-OES)

ICP-OES was used to measure Si concentration in silicified cells. 20 x10^6 cells were washed with water and dried under vacuum for 7 days and then mineralized in aqua regia (1:3 mixture of ultrapure HNO_3 and HCl) with a Digi prep MS SCP Science block digester at 95°C for 4 hours. The digested samples were diluted and passed through 0.45 μm filter. The concentration of Si was then measured using a PerkinElmer Optima 5300DV ICP-OES, with a detection limit of < 0.5 mg/L. ICP-OES is calibrated with a five-point calibration curve. QA/QC measurements were also obtained to ensure quality results.

Silicified cell degradation in simulated endosomal solution

Twenty million silicified cells were suspended in 4 mL simulated endosomal solution containing acetate buffer, pH 5.2 (Poly Scientific R&D Corp., Bayshore, NY, USA) and 20% FBS at room temperature under rotation for 3 days. After incubation, the cells were rinsed with water and then dried under vacuum for 7 days. The Si content of silicified cells pre and post treatment was measured using ICP-OES.

Proliferation assays

Native and silicified cells, with/without PEI coating, were assessed for cell growth using the CellTiter-Glo 2.0 Assay. Briefly, cells were seeded at a density of 100,000 cells/mL in culture media in white opaque 96-well plates. After 24 hours, CellTiter-Glo 2.0 Reagent was added to each well, and following a 10-minute incubation, luminescence was determined using a BioTek microplate reader. Percent cell viability was calculated relative to control, non-treated cells.

Preparation of mesoporous silica nanoparticles (MSN)

A mixture of water (100 mL), ethanol (40 mL), sodium hydroxide (NaOH, 2M, 0.75 mL) and cetyltrimethylammonium bromide (CTAB, 0.640 g) was heated to 70 °C under vigorous stirring (750 rpm) in a round bottom flask immersed in an oil bath. Afterwards, tetraethyl orthosilicate (TEOS, 1 mL) was added dropwise to the solution. The TEOS was allowed to undergo a series of hydrolysis condensation reactions for 2 hours to yield silica CTAB-templated silica nanoparticles. The particles were then isolated by centrifugation (2000 g, 20 minutes) and then washed with MeOH three times. The surfactant removal was performed by suspending the nanoparticles in a solution of 0.45 g/L ammonium nitrate in ethanol and

stirring at 60 °C for 20 minutes. Finally, the template-free MSN were consecutively washed twice with water and ethanol and stored suspended in ethanol. MSN (0.5 mg) were rinsed twice with water and then suspended in 1mL of 0.2 mg/mL PEI in PBS solution. After 10 minutes rotation at room temperature to allow PEI binding on the MSN surface, the MSN with PEI coating (MSN-PEI) were then rinsed with PBS twice. MSN-PEI (0.87 mg) were suspended in 20 μL of 2mg/mL CPG in double distilled water solution. After 10 minutes incubation at room temperature, 25 μL of 1mg/mL MPL in DMSO solution was added and incubated another 10 minutes. MSN-PEI-CPG-MPL particles were then centrifuge at 20000 rcf for 5 minutes to remove extra free ligand, and then resuspended and stored in 1 mL PBS. These conditions result in similar CpG and MPL dose content to vaccine cells.

In vitro DC functional studies

Bone marrow-derived or human ascites DCs were seeded in 12-well plates at a density of 1×10^5 cells per well. After 24 h, the media was removed and replaced with 2 mL of fresh complete media supplemented with 100,000 Si-PEI-CpG-MPL (or irradiated PEI-CpG-MPL) ID8ova or human cancer cells for 24 or 72 hours as indicated. Alternatively, DC were incubated with Si-LPS or Si-MPL ID8ova cells for 72 hours. Irradiated cells were suspended in PBS in microfuge tubes at 3×10^6 cells/mL and exposed to 100 Gy using a Faxitron Multirad Irradiator at 22rV, 15 mA, 48 Gy/min. DCs were collected using 3mM EDTA. The suspended cells were centrifuged, washed with PBS containing 1% BSA, and labeled with fluorescent antibodies specific for CD11c and either co-stimulatory molecules or SIINFEKL-H2-k^b. Cells were analyzed using the Becton Dickinson Fortessa or Calibur Flow Cytometer.

Vaccination of mice with Si-tumour cells

Tumour-bearing or naïve female FVB or albino C57BL/6 mice were vaccinated intraperitoneally with irradiated (100 Gy using a Faxitron Multirad Irradiator at 225V, 15 mA, 48 Gy/min; or a Cs-137 gamma irradiator with a dose rate of 63 cGy/min) or silicified BR5-Akt (or BR5-Akt-Luc2 for vaccine viability analysis or ID8ova) cells (with TLR ligands as indicated) using doses of 3×10^4, 3×10^5, 3×10^6, or 3×10^7 Si-cells/ mouse in 200 μl of PBS at the indicated schedules. Control vaccines, all containing CpG and MPL, included no antigen MSN, silicified leukocytes (splenocytes from naïve mice), and oxidized cell lysate. Cell lysate was prepared by incubating BR5-Akt cells in 60 μM hypochlorous acid (HOCl) in PBS for 1 hour at 37°C, followed by extensive PBS washing and five freeze-thaw cycles using dry ice and a 37°C water bath [7,48,49]. Alternatively, mice were vaccinated subcutaneously (SC) with 3×10^6 silicified BR5-Akt cells by scruffing the skin at the back of their neck and injecting an equivalent volume into the loose fold of skin. Mice that cleared all tumour cells based on IVIS Spectrum bioluminescent imaging were re-challenged with 2×10^5 BR5-Akt-Luc2 cancer cells at a later date, as indicated for each study. All control (no Tx) mice received sham PBS injections (200 μl/mouse). Single agent or combination therapy with cisplatin used IP administration of *cis*-Diamineplatinum (II) dichloride (Sigma-Aldrich) on Day 9 at 2 mg/kg in physiological saline.

Preparation of ascites-derived tumour vaccines

To prepare vaccine using murine tumour (ascites) cells, peritoneal fluid was collected from mice with late-stage BR5-Akt cancer. The intact peritoneal cavity was exposed and ascites, as well as 2 peritoneal wash samples with cold PBS, were collected using an 18G needle and 5mL syringe inserted in the hypogastric region and positioned towards the cecum. In addition, ascites fluid was collected from patients with a diagnosis of ovarian cancer at the time of surgical debulking in accordance with approved IRB Protocol #UNM INST 1509, entitled "Single Institution (UNM) Prospective Laboratory Study of Cancer and Immune Cells in the Ascites Fluid of Ovarian Cancer Patients to Test Alternative Therapies." Human specimens were de-identified prior to transfer for research purposes. To isolate peritoneal cells, human or mouse ascites were centrifuged at 1400 RPM for 5 minutes, after which the supernatant was removed, and RBCs were removed using ACK lysis buffer. Tumour cells were enriched using a 37 μm reversible strainer. EpCAM$^+$ populations were evaluated by flow cytometry. Cells were then silicified and surface modified as previously described.

Adoptive transfer of CD8$^+$ T cells

Peritoneal washings were collected from tumour bearing vaccinated (Day 33 post tumour challenge) and control (tumour and vaccine naïve) FVB mice as described above. Cells were enriched for CD8+ T-cells using the negative selection mouse CD8a$^+$ T Cell Isolation MACS Cell Separation Kit (Miltenyi Biotec). Purification was confirmed post separation using flow cytometry. Cells were resuspended in cold PBS and adaptively transferred IP ($2x10^5$cells/mouse) to tumour and vaccine naïve FVB mice. Control mice received sterile PBS IP. 24 hours after transfer of CD8$^+$ T cells, recipient mice were challenged with IP BR5-Akt-Luc2$^+$ tumour cells ($2x10^5$/mouse). Mice where then monitored for tumour progression using luminescence on IVIS Spectrum In Vivo Imaging System (PerkinElmer).

Imaging tumour burden

For *in vivo* monitoring of tumour burden, mice with BR5-Akt-Luc2 tumours were administered 150 mg luciferin/kg by intraperitoneal injection, with a 10-minute delay before imaging. Mice were then anesthetized using 2.5% isoflurane, and 2D/3D bioluminescence images were acquired using the Xenogen IVIS Spectrum animal imager (PerkinElmer). ROI measurements of total flux (photons/sec) were acquired using Living Image Software (Perkin Elmer).

Murine tissue/cell collection

All mice were euthanized in accordance with Institutional Animal Care and Use Committee (IACUC) at the University of New Mexico (Albuquerque NM). Spleens were mechanically dissociated, and RBC were eliminated using ACK or BD Pharm Lyse. Blood was collected by retro-orbital withdrawal using EDTA or heparin to prevent blood clotting. Omentum, peritoneal tumour, lungs, gut, brain, and kidneys were dissected out and fixed in 10% buffered formalin. Tissues were embedded in paraffin, sectioned and stained with H&E by the University of New Mexico Health Science Center Histology and Molecular Pathology Shared Resource. Bright-field images were acquired using a World Precision Instruments,

Inc. dissection microscope equipped with a Sony CCD progressive scan color camera (World Precision Instruments, Sarasota, FL, USA).

Biodistribution of vaccine

To track vaccine cells, BR5-Akt cancer cells were first incubated with Cy3-labeled MSN for 16 hours. Cells were then washed to remove free MSN and following silicification, 3×10^6 Si-PEI-CpG-MPL cells in 200μL PBS were IP administered to FVB mice four days post IP tumour challenge. Twenty-four hours later, mice were euthanized, and peritoneal tissues were frozen in optimal cutting temperature (OCT) compound. Following sectioning, tissues were fixed in ice-cold acetone for 15 minutes, labeled with anti-mouse CD11c FITC antibody and mounted in Prolong Gold Mounting Media containing DAPI. Images were acquired using a 63X/1.4NA oil objective in sequential scanning mode using a Leica TCS SP8 confocal microscope. To study in vivo tissue biodistribution, CTFR-labeled vaccine cells were administered to FVB mice 4 days post tumour challenge. On days 5 and 6, organs were isolated from mice (n=2-3/group) and the IVIS Spectrum was used to measure fluorescent intensities.

Immune cell phenotyping

Single-cell suspensions were first blocked with Fc receptor blockers (1 μg anti-CD16/CD32 (clone 2.4G2) and 1 μg mouse IgG. Next, samples were surface stained with conjugated primary antibodies (1:250 dilution) at room temperature for 30 minutes in the dark. Samples were then stained with LIVE/DEAD™ Fixable Aqua Dead Cell Stain for 15 min at room temperature in the dark. For intracellular cytokine analysis, cells were stimulated using eBioscience Cell Stimulation Cocktail (500X) plus Protein Transport Inhibitors Cocktail (500X) for 4 hours in RMPI complete media. Cell permeabilization for intracellular staining was done using the eBioscience™ FoxP3 / Transcription Factor Staining Buffer Set. Phenotyping was performed on stained cells using the Attune NxT Flow Cytometer and analyzed using FlowJo (10.6) (Becton, Dickinson and Company).

Cytokine analysis

Neat peritoneal fluid from mice bearing BR5-Akt tumours at various stages of progression, with no treatment or following treatment with dehydrated vaccine, was collected and stored at −80°C. Samples were evaluated using a custom Milliplex MAP Mouse High Sensitivity T cell Panel using the Luminex MAGPIX System (Sigma Aldrich) without dilution as decribed by the vendor.

Blood metabolite measurements

Anti-coagulated blood metabolites and complete blood counts were measured on Day 18 or 19 using the Vetscan VS2 Analyzer and Comprehensive or Partial Diagnostic Profile discs (Abaxis, Union City, CA, USA) as described by the vendor.

Statistical Analysis

Measurements in this study were obtained from distinct samples. Graphpad Prism was used to perform statistical analysis. Kaplan-Meier survival curves were analyzed using Log-rank

Mantel-Cox and Match SPSS and SAS tests for two and multiple group comparisons, respectively. For tumour burden comparisons, multiple t-tests assuming all rows are sampled from populations with the same scatter and correction for multiple comparisons using the Holm-Sidak method were used. Column statistics were analyzed using unpaired, two-tailed parametric t tests with equal SD. Graphs include means and error bars, with the latter representing standard deviation or standard error of mean if indicated.

Reporting Summary

Further information on research design is available in the Nature Research Reporting Summary linked to this article.

Data availability

All figures have associated raw data. Graphpad prism tumor burden files are included as source data.

Code availability

No custom codes or mathematical algorithms are used in this study.

Extended Data
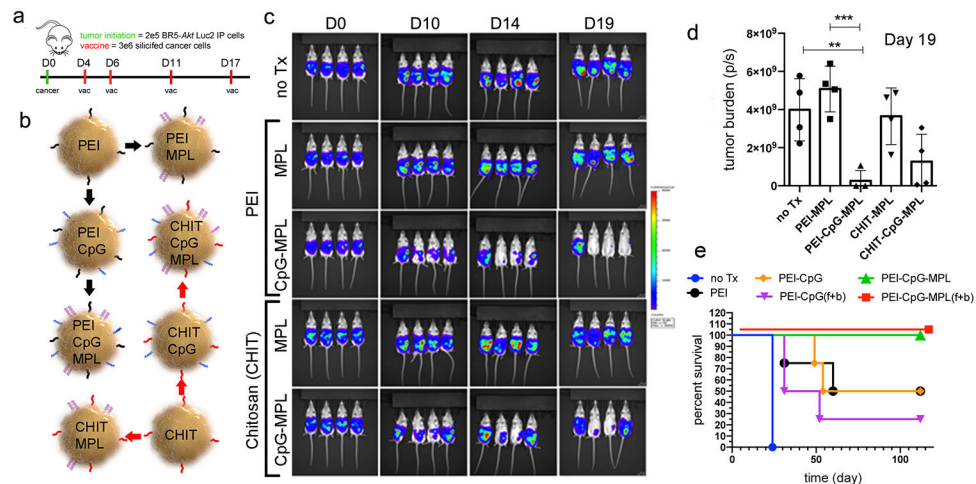
ED Fig. 1. Therapeutic efficacy of single vs dual TLR ligand vaccines
a) Timeline for BR5-Akt-Luc2 cancer cell and vaccine administration. b) Chitosan (CHIT) or polyethylimine (PEI) vaccine formulations containing MPL; CpG; or MPL plus CpG. c) IVIS bioluminescence images of FVB mice over time. d) Average tumor burden (photons/ second; p/s) of each group shown in "c" on Day 19 (Unpaired, two-tailed, parametric t-tests, SD error bars). e) Kaplan-Meier survival curves for mice treated with silicified (Si)-PEI cells coated with CpG, or CpG and MPL. f = free, and b = bound TLR ligand; (n=4/group, Log-rank Mantel-Cox: p<0.0001 with symbols to the right on the survival curve representing comparisons with no treatment (no Tx) controls and the symbol on the purple line comparing the CpG vs CpG/MPL (f+b) groups. * p<0.05, **p<0.01, p<0.001.
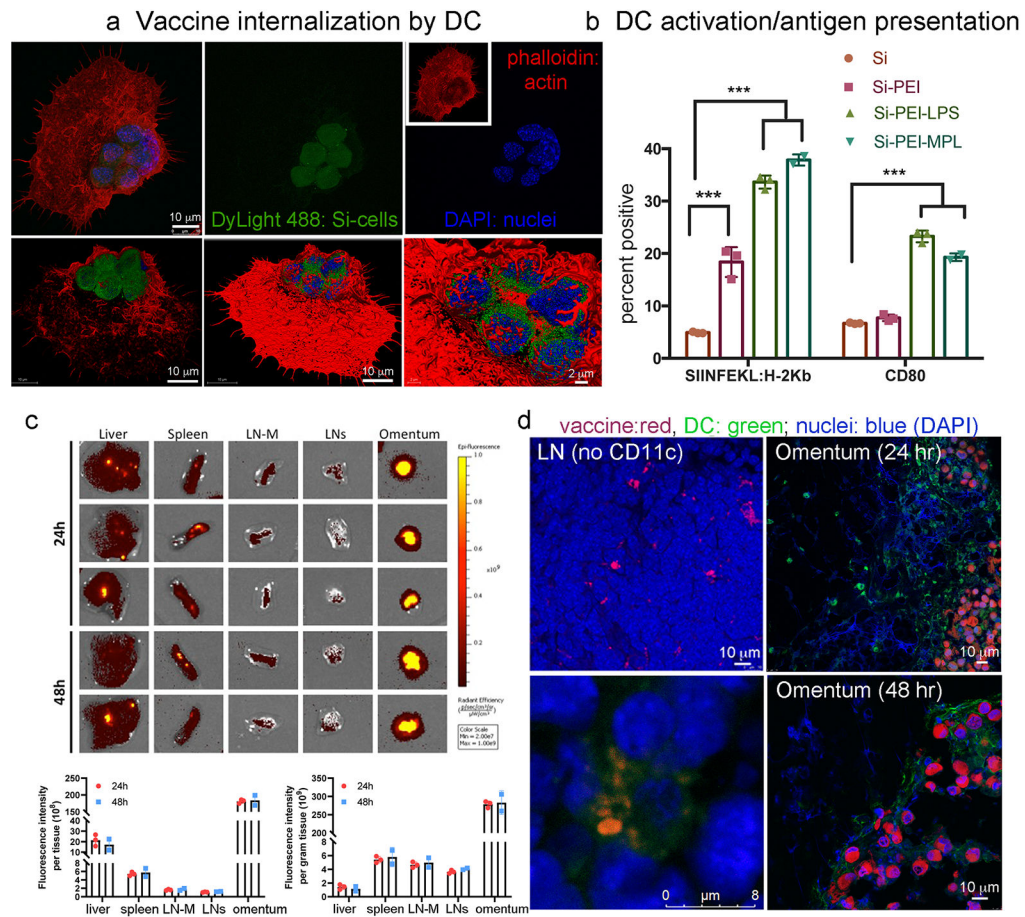
ED Fig. 2. Bone marrow-derived dendritic cell (BMDC) activation and internalization of silicified (Si) cells

a) 2D and 3D confocal images show five internalized Si-LPS-ID8ova cells (visualized via internalized DyLight 488-labeled nanoparticles) in a single BMDC. b) Flow cytometry analysis of SIINFEKL MHC-I (H-2Kb) presentation and surface expression of CD80 in BMDC incubated with Si cells presenting null, PEI, or PEI plus LPS or MPL for 24 hours (n=3/group; ***p<0.001). c) Cell Trace Far Red-labeled vaccine cells were predominately located in filtering and lymphatic organs (LN-M: mesenteric; LNs: Inguinal and axillary) 24 and 48 hours post IP injection in tumor-bearing mice (n= 2-3 biological replicates). d) Fluorescent vaccine cells (red; Cy3) were located in peritoneal lymph nodes and the omentum, predominately in DC-rich areas, 24-48 hours post IP injection in naïve mice (green, right; CD11c FITC; blue nuclei, DAPI). Unpaired, two-tailed, parametric t-tests, SD error bars.
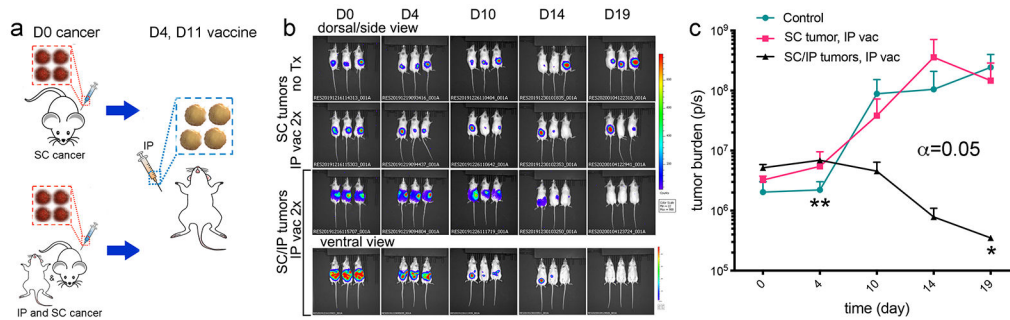
ED Fig. 3. Therapeutic vaccination in the tumour microenvironment enables systemic immunity
a) Experimental design and timeline (n=3). b) IVIS bioluminescent images of BR5-Akt-Luc2 tumor growth. c) Graph of tumor burden (photons/sec) across time by treatment group (no treatment (no Tx) and tumor location. Intraperitoneal (IP) vaccination of mice bearing both subcutaneous (SC) and IP tumors cleared established tumors in both locations while mice with only SC tumors continued to display tumor growth (n=3/group, Holm-Sidak multiple comparison; individual animal curves in SI). **p<0.01.
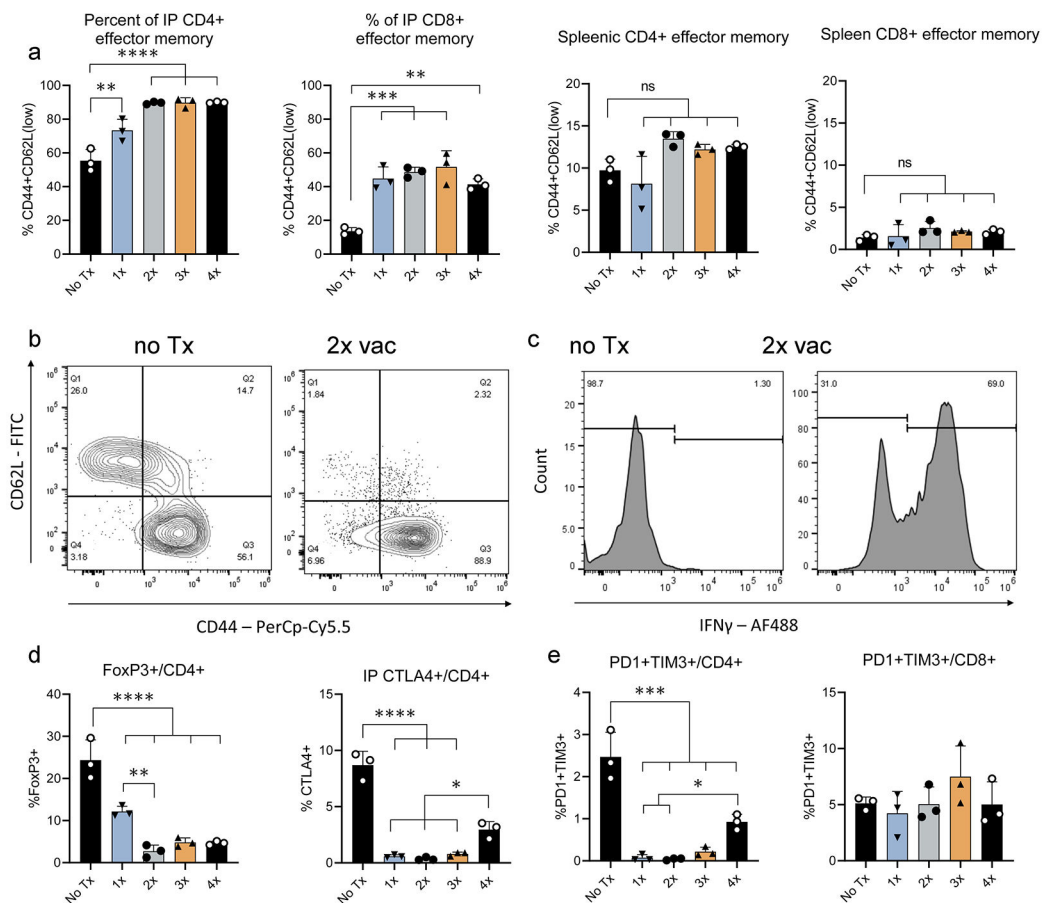
ED Fig. 4. Vaccination activates T cells in the tumour microenvironment
To test the effect of treatment number on IP immune responses, IP cells were collected and analyzed for activation and functional status using flow cytometry on Day 19 following

tumor challenge in mice vaccinated 1x, 2x, 3x, 4x or those receiving no treatment (PBS; no Tx) on days 4, 6,11 and 17. a) Proportion of IP CD4 and CD8 cells with effector memory phenotypes (CD44+CD62L^{low}). b) Representative dot plot for effector memory CD4+ IP cells (CD44 vs CD62L. c) Representative plot for IFNγ expression by IP CD4+ cells from with no vaccination vs 2x vaccination. d) Proportion of IP CD4+ cells expressing the regulatory markers CTLA4 and FoxP3. e) Proportion of CD4+ and CD8+ IP cells expressing PD1 and Tim3. n=3 biological replicates; unpaired, two-tailed, parametric t-tests, SD error bars, *p<0.05, **p<0.01, ***p<0.001.
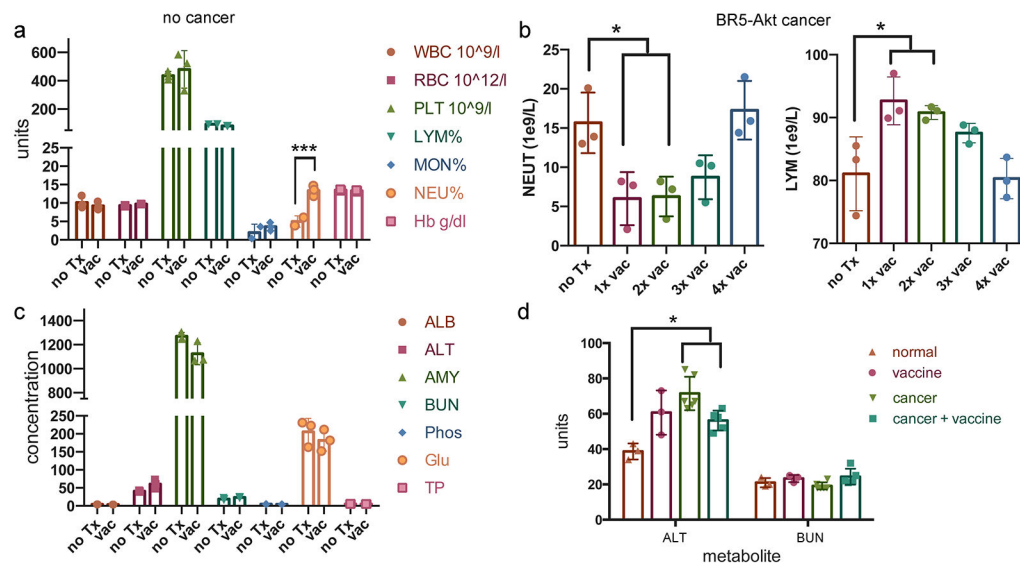
ED Fig. 5. CBC and blood metabolite analysis supports vaccine safety
Tumor naïve (a,c) or cancer challenged (b,d) FVB mice (n=3 biological replicates; unpaired, two-tailed, parametric t-tests) were vaccinated 1-4x. Graphs show cell counts by population and blood metabolites obtained using the Abaxis VetScan System and piccolo metabolite discs. *p<0.05, ***p<0.001.

Supplementary Material

Refer to Web version on PubMed Central for supplementary material.

Acknowledgements

References

1. Sharma P & Allison JP Immune checkpoint targeting in cancer therapy: toward combination strategies with curative potential. Cell 161, 205–214, doi:10.1016/j.cell.2015.03.030 (2015). [PubMed: 25860605]

2. Srivatsan S et al. Allogeneic tumour cell vaccines: the promise and limitations in clinical trials. Hum Vaccin Immunother 10, 52–63, doi:10.4161/hv.26568 (2014). [PubMed: 24064957]

3. Chiang CL, Coukos G & Kandalaft LE Whole Tumour Antigen Vaccines: Where Are We? Vaccines (Basel) 3, 344–372, doi:10.3390/vaccines3020344 (2015). [PubMed: 26343191]

4. Sahin U & Tureci O Personalized vaccines for cancer immunotherapy. Science 359, 1355–1360, doi:10.1126/science.aar7112 (2018). [PubMed: 29567706]

5. Kantoff PW et al. Sipuleucel-T immunotherapy for castration-resistant prostate cancer. N Engl J Med 363, 411–422, doi:10.1056/NEJMoa1001294 (2010). [PubMed: 20818862]

6. Hollingsworth RE & Jansen K Turning the corner on therapeutic cancer vaccines. NPJ Vaccines 4, 7, doi:10.1038/s41541-019-0103-y (2019). [PubMed: 30774998]

7. Chiang CL et al. A dendritic cell vaccine pulsed with autologous hypochlorous acid-oxidized ovarian cancer lysate primes effective broad antitumour immunity: from bench to bedside. Clin Cancer Res 19, 4801–4815, doi:10.1158/1078-0432.CCR-13-1185 (2013). [PubMed: 23838316]

8. Kandalaft LE et al. A Phase I vaccine trial using dendritic cells pulsed with autologous oxidized lysate for recurrent ovarian cancer. J Transl Med 11, 149, doi:10.1186/1479-5876-11-149 (2013). [PubMed: 23777306]

9. Kamigaki T et al. Immunotherapy of autologous tumour lysate-loaded dendritic cell vaccines by a closed-flow electroporation system for solid tumours. Anticancer Res 33, 2971–2976 (2013). [PubMed: 23780988]

10. Sarivalasis A et al. A Phase I/II trial comparing autologous dendritic cell vaccine pulsed either with personalized peptides (PEP-DC) or with tumour lysate (OC-DC) in patients with advanced high-grade ovarian serous carcinoma. J Transl Med 17, 391, doi:10.1186/s12967-019-02133-w (2019). [PubMed: 31771601]

11. Pattillo RA, Komaki R, Reynolds M & Robles J Bacillus Calmette-Guerin immunotherapy in ovarian cancer. J Reprod Med 33, 41–45 (1988). [PubMed: 3351805]

12. Nishida S et al. Immune adjuvant therapy using Bacillus Calmette-Guerin cell wall skeleton (BCG-CWS) in advanced malignancies: A phase 1 study of safety and immunogenicity assessments. Medicine (Baltimore) 98, e16771, doi:10.1097/MD.0000000000016771 (2019). [PubMed: 31415377]

13. Walker JJ, Spear JR & Pace NR Geobiology of a microbial endolithic community in the Yellowstone geothermal environment. Nature 434, 1011–1014, doi:10.1038/nature03447 (2005). [PubMed: 15846344]

14. Hamm CE et al. Architecture and material properties of diatom shells provide effective mechanical protection. Nature 421, 841–843, doi:10.1038/nature01416 (2003). [PubMed: 12594512]

15. Kaehr B et al. Cellular complexity captured in durable silica biocomposites. Proc Natl Acad Sci U S A 109, 17336–17341, doi:10.1073/pnas.1205816109 (2012). [PubMed: 23045634]

16. Meraz IM et al. Multivalent presentation of MPL by porous silicon microparticles favors T helper 1 polarization enhancing the anti-tumour efficacy of doxorubicin nanoliposomes. PLoS One 9, e94703, doi:10.1371/journal.pone.0094703 (2014). [PubMed: 24736547]

17. Savage DJ, Liu X, Curley SA, Ferrari M & Serda RE Porous silicon advances in drug delivery and immunotherapy. Curr Opin Pharmacol 13, 834–841, doi:10.1016/j.coph.2013.06.006 (2013). [PubMed: 23845260]

18. Meraz IM et al. Activation of the inflammasome and enhanced migration of microparticle-stimulated dendritic cells to the draining lymph node. Mol Pharm 9, 2049–2062, doi:10.1021/mp3001292 (2012). [PubMed: 22680980]

19. Melisi D et al. Toll-Like Receptor 9 Agonists for Cancer Therapy. Biomedicines 2, 211–228, doi:10.3390/biomedicines2030211 (2014). [PubMed: 28548068]

20. Lynn GM et al. In vivo characterization of the physicochemical properties of polymer-linked TLR agonists that enhance vaccine immunogenicity. Nat Biotechnol 33, 1201–1210, doi:10.1038/nbt.3371 (2015). [PubMed: 26501954]

21. Blander JM Phagocytosis and antigen presentation: a partnership initiated by Toll-like receptors. Ann Rheum Dis 67 Suppl 3, iii44–49, doi:10.1136/ard.2008.097964 (2008). [PubMed: 19022813]

22. Kumar S, Sunagar R & Gosselin E Bacterial Protein Toll-Like-Receptor Agonists: A Novel Perspective on Vaccine Adjuvants. Front Immunol 10, 1144, doi:10.3389/fimmu.2019.01144 (2019). [PubMed: 31191528]

23. Ma YF & Yang YW Delivery of DNA-based cancer vaccine with polyethylenimine. Eur J Pharm Sci 40, 75–83, doi:10.1016/j.ejps.2010.02.009 (2010). [PubMed: 20304049]

24. Hu K et al. An ocular mucosal administration of nanoparticles containing DNA vaccine pRSC-gD-IL-21 confers protection against mucosal challenge with herpes simplex virus type 1 in mice. Vaccine 29, 1455–1462, doi:10.1016/j.vaccine.2010.12.031 (2011). [PubMed: 21185849]

25. Kuai R et al. Dual TLR agonist nanodiscs as a strong adjuvant system for vaccines and immunotherapy. J Control Release 282, 131–139, doi:10.1016/j.jconrel.2018.04.041 (2018). [PubMed: 29702142]

26. De Nardo D, De Nardo CM, Nguyen T, Hamilton JA & Scholz GM Signaling crosstalk during sequential TLR4 and TLR9 activation amplifies the inflammatory response of mouse macrophages. J Immunol 183, 8110–8118, doi:10.4049/jimmunol.0901031 (2009). [PubMed: 19923461]

27. Moghimi SM et al. A two-stage poly(ethylenimine)-mediated cytotoxicity: implications for gene transfer/therapy. Mol Ther 11, 990–995, doi:10.1016/j.ymthe.2005.02.010 (2005). [PubMed: 15922971]

28. McConnell KI et al. Reduced Cationic Nanoparticle Cytotoxicity Based on Serum Masking of Surface Potential. J Biomed Nanotechnol 12, 154–164, doi:10.1166/jbn.2016.2134 (2016). [PubMed: 27301181]

29. Doyle SE et al. Toll-like receptors induce a phagocytic gene program through p38. J Exp Med 199, 81–90, doi:10.1084/jem.20031237 (2004). [PubMed: 14699082]

30. Cole GA Interferon-gamma ELISPOT assay for the quantitative measurement of antigen-specific murine CD8+ T-cells. Methods Mol Biol 302, 191–204, doi:10.1385/1-59259-903-6:191 (2005). [PubMed: 15937353]

31. Koster BD et al. Autologous tumour cell vaccination combined with systemic CpG-B and IFN-alpha promotes immune activation and induces clinical responses in patients with metastatic renal cell carcinoma: a phase II trial. Cancer Immunol Immunother 68, 1025–1035, doi:10.1007/s00262-019-02320-0 (2019). [PubMed: 30852622]

32. Giuntoli RL 2nd et al. Ovarian cancer-associated ascites demonstrates altered immune environment: implications for antitumour immunity. Anticancer Res 29, 2875–2884 (2009). [PubMed: 19661290]

33. Lee CH, Wu CL, Tai YS & Shiau AL Systemic administration of attenuated Salmonella choleraesuis in combination with cisplatin for cancer therapy. Mol Ther 11, 707–716, doi:10.1016/j.ymthe.2005.01.008 (2005). [PubMed: 15851009]

34. Burgdorf S & Kurts C Endocytosis mechanisms and the cell biology of antigen presentation. Curr Opin Immunol 20, 89–95, doi:10.1016/j.coi.2007.12.002 (2008). [PubMed: 18249105]

35. Savina A et al. NOX2 controls phagosomal pH to regulate antigen processing during crosspresentation by dendritic cells. Cell 126, 205–218, doi:10.1016/j.cell.2006.05.035 (2006). [PubMed: 16839887]

36. Lee YK et al. Kinetics and Chemistry of Hydrolysis of Ultrathin, Thermally Grown Layers of Silicon Oxide as Biofluid Barriers in Flexible Electronic Systems. ACS Appl Mater Interfaces 9, 42633–42638, doi:10.1021/acsami.7b15302 (2017). [PubMed: 29178781]

37. Choi E & Kim S Surface pH buffering to promote degradation of mesoporous silica nanoparticles under a physiological condition. J Colloid Interface Sci 533, 463–470, doi:10.1016/j.jcis.2018.08.088 (2019). [PubMed: 30172772]

38. Tanyi JL et al. Personalized cancer vaccine effectively mobilizes antitumour T cell immunity in ovarian cancer. Sci Transl Med 10, doi:10.1126/scitranslmed.aao5931 (2018).

39. https://www.cancer.gov/about-cancer/treatment/clinical-trials/intervention/bcg-vaccine.

40. Stump CT et al. Remission-Stage Ovarian Cancer Cell Vaccine with Cowpea Mosaic Virus Adjuvant Prevents Tumour Growth. Cancers (Basel) 13, doi:10.3390/cancers13040627 (2021).

41. Prasad S et al. Polymer nanoparticles containing tumour lysates as antigen delivery vehicles for dendritic cell-based antitumour immunotherapy. Nanomedicine 7, 1–10, doi:10.1016/j.nano.2010.07.002 (2011). [PubMed: 20692374]

42. Chiang CL et al. Optimizing parameters for clinical-scale production of high IL-12 secreting dendritic cells pulsed with oxidized whole tumour cell lysate. J Transl Med 9, 198, doi:10.1186/1479-5876-9-198 (2011). [PubMed: 22082029]

43. Morehead LC & Cannon MJ Further clinical advancement of dendritic cell vaccination against ovarian cancer. Ann Res Hosp 2, doi:10.21037/arh.2018.08.02 (2018).

44. Nair-Gupta P et al. TLR signals induce phagosomal MHC-I delivery from the endosomal recycling compartment to allow cross-presentation. Cell 158, 506–521, doi:10.1016/j.cell.2014.04.054 (2014). [PubMed: 25083866]

45. Xing D & Orsulic S A mouse model for the molecular characterization of brca1-associated ovarian carcinoma. Cancer Res 66, 8949–8953, doi:10.1158/0008-5472.CAN-06-1495 (2006). [PubMed: 16982732]

46. Roby KF et al. Development of a syngeneic mouse model for events related to ovarian cancer. Carcinogenesis 21, 585–591 (2000). [PubMed: 10753190]

47. Higuchi T et al. CTLA-4 Blockade Synergizes Therapeutically with PARP Inhibition in BRCA1-Deficient Ovarian Cancer. Cancer Immunol Res 3, 1257–1268, doi:10.1158/2326-6066.CIR-15-0044 (2015). [PubMed: 26138335]

48. Chiang CL, Ledermann JA, Rad AN, Katz DR & Chain BM Hypochlorous acid enhances immunogenicity and uptake of allogeneic ovarian tumour cells by dendritic cells to cross-prime tumour-specific T cells. Cancer Immunol Immunother 55, 1384–1395, doi:10.1007/s00262-006-0127-9 (2006). [PubMed: 16463039]

49. Chiang CL et al. Day-4 myeloid dendritic cells pulsed with whole tumour lysate are highly immunogenic and elicit potent anti-tumour responses. PLoS One 6, e28732, doi:10.1371/journal.pone.0028732 (2011). [PubMed: 22194898]
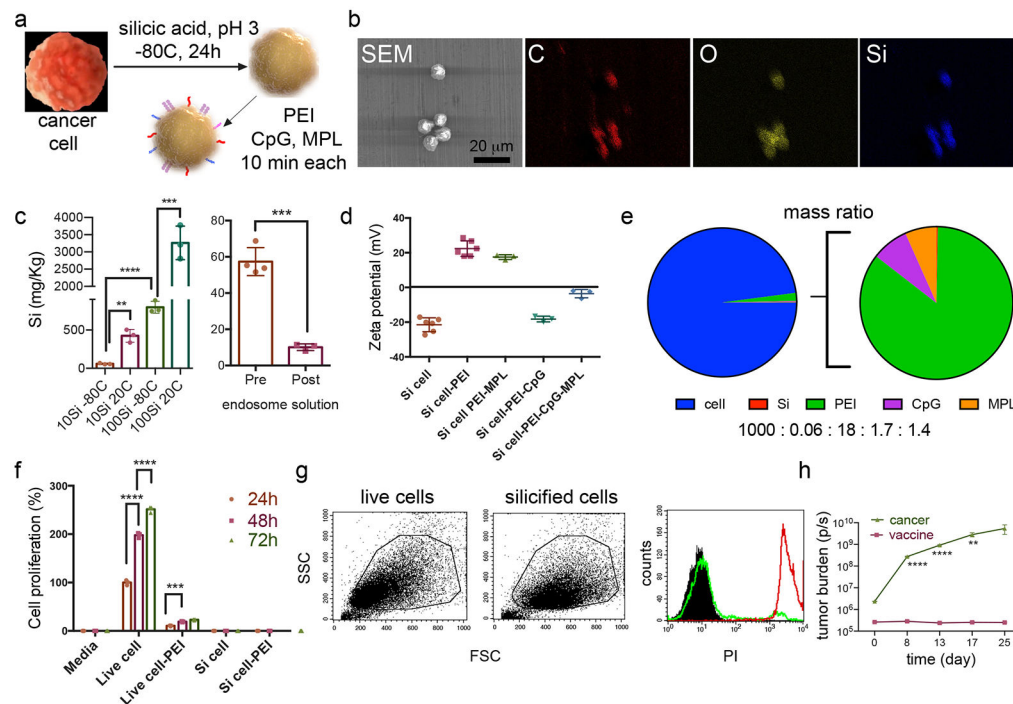
Fig. 1 |.

Characterization of silicified cancer cells. a) Cryo-silicification and adsorption of PAMPs to cancer cells. b) Confirmation of Si content in silicified BR5-*Akt* tumour cells using SEM and energy dispersive X-ray analysis of carbon (C), oxygen (O), and silicon (Si). c) ICP-OES analysis of Si content in BR5-*Akt* cells silicified using either 10 or 100 mM silicic acid solution for 24 hours at 20°C or −80°C (20°C vs 80°C at 10Si p=0.0017 and 100Si p=0.001; centre values 59, 424, 798 and 3263; SD error bars.7; n=3 biological replicates; unpaired, two-tailed, parametric t-tests); and Si content in 10 mM cryo-silicified cells before and after 72 hours in simulated endosomal fluid (p=0.0002; centre values 57 and 10, SD error bars; n=3-4 biological replicates; unpaired, two-tailed, parametric t-test). d) Zeta potential analysis of silicified cells with different surface modifications (n=3-6 biological replicates/group; centre values are −22, 22, 17, −18, and −4; SD error bars). e) Pie charts showing Si-PEI-CpG-MPL cell composition by mass ratio. f) Cell-Glo proliferation assay of live or silicified BR5-*Akt* cells, with and without a 10 minute immersion in 0.2 mg/mL PEI measured at 24, 48 and 72 hours (n=5 biological replicates; p=0.0002 unpaired, two-tailed, parametric t-test for 24 vs 48 hr for live cells with PEI; for live cell and live cell PEI, centre values are 22, 44, and 55; SD error bars). g) Flow cytometry scatter dotplots of live or silicified BR5-*Akt* cells showing change in size (FSC) with silicification and histogram of cells before or after staining with propidium iodide (PI) to demonstrate that silicified cells are non viable (n=3 biological replicates). h) Tumour burden over time based on IVIS bioluminescence of FVB mice IP injected on day 0 with either live (cancer challenged) or silicified (vaccine only) BR5-A*kt*-Luc2 cells (n=3/group; p=0.0013 day 13; Holm-Sidak multiple comparison; individual animal curves in SI). *p<0.05, **p<0.01, ***p<0.001.
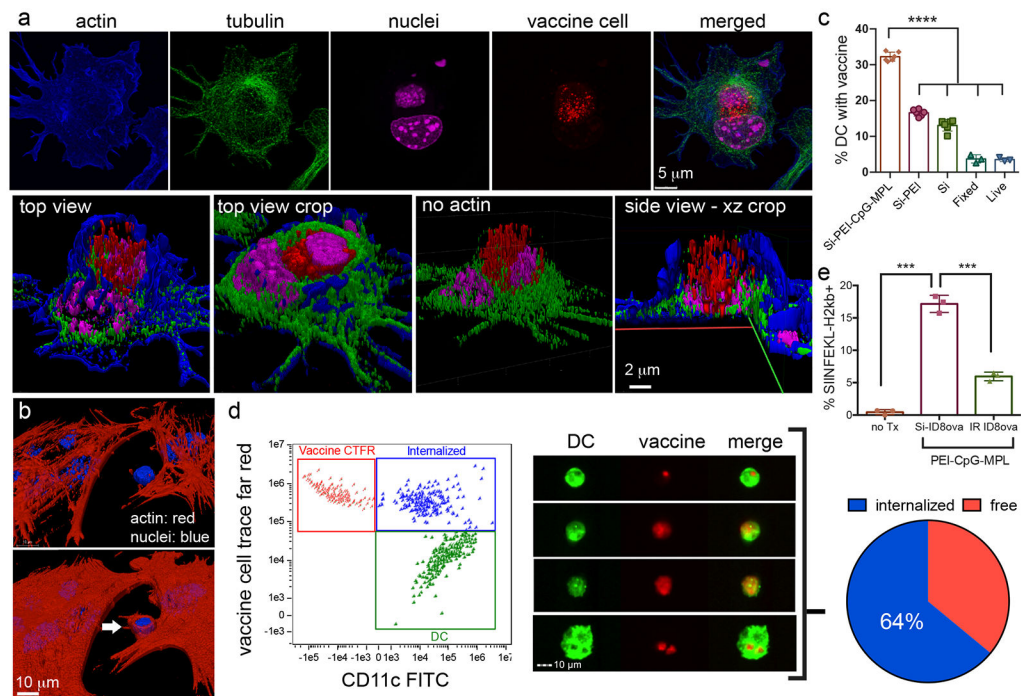
Fig.2 |.

Surface functionalization enhances DC uptake and activation *in vitro*. a-b) 2D and surface-rendered 3D fluorescent confocal micrographs showing internalization and intracellular location of silicified tumour cells following 1 hour incubation with GM-CSF-matured BMDC. a) Actin fluorescence is shown at 3 threshold levels for inside and surface views. The white arrow points to active phagocytosis. b) Tumour cells were pre-incubated with fluorescent nanoparticles prior to silicification to distinguish vaccine cells from DC. c) Flow cytometry analysis of DC uptake of silicified BR5-*Akt* cells presenting no TLR ligands (Si); PEI; or PEI, CpG and MPL (n=3-6 biological replicates; unpaired, two-tailed, parametric t-tests; centres 32, 17, 13, 4, and 4; SD error bars) d) Amnis Imagestream imaging cytometry analysis of vaccine (Cell Trace Far Red; red) internalization by BMDC (5:1 for 24 hours; anti-CD11c mAb FITC; green) (n=3). e) Flow cytometry analysis of MHC I presentation of tumour antigen (SIINFEKL-H2Kb) on DC 72 hours after addition of ID8ova vaccine cells or control irradiated ID8ova cells (n=3 biological replicates; unpaired, two-tailed, parametric t-tests; centres 0.4, 17.2, and 6.0; SD error bars). ****p<0.0001
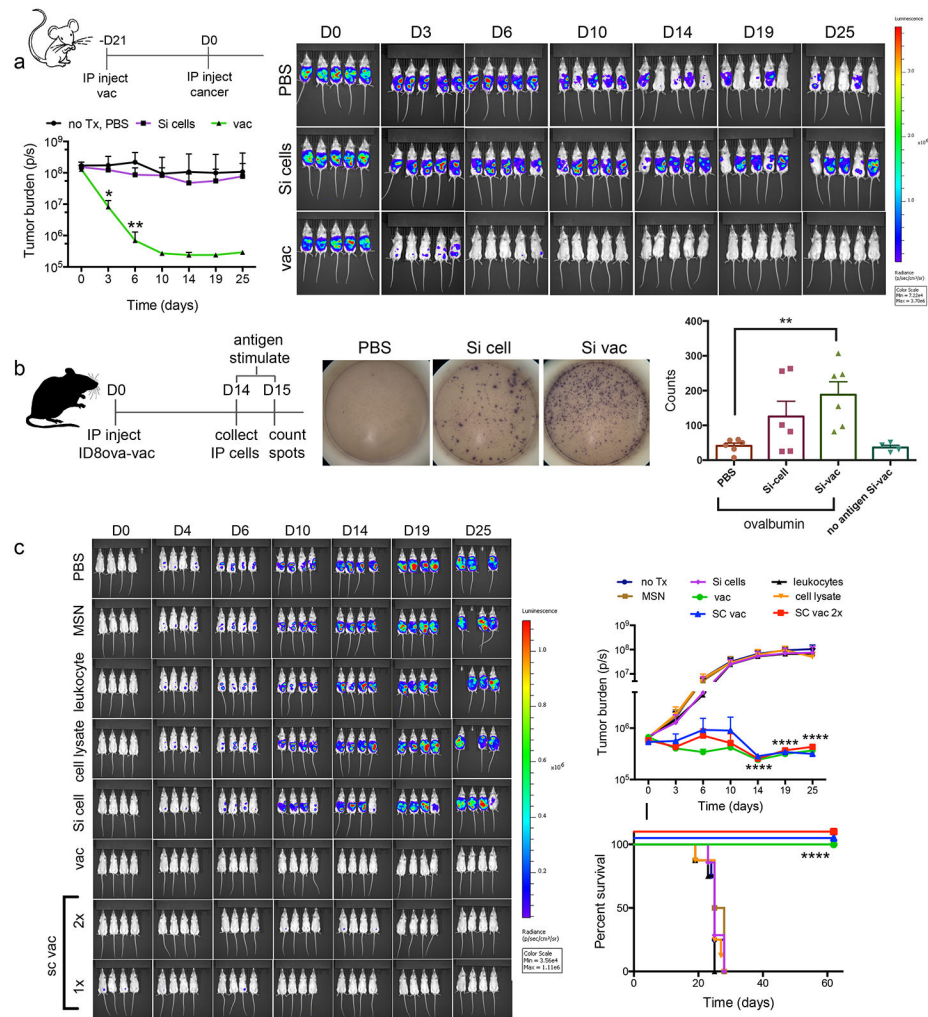
Fig.3 |.

Treatment with silicified cells induces a protective immune response *in vivo.* a) Tumour engraftment was evaluated in albino C57BL/6 challenged with ID8ova-Luc2 cells 21 days following IP administration of vaccine (n=10/group; no Tx vs vaccinated p= 0.03 and 0.005 at Days 3 and 6, Holm-Sidak multiple comparison). b) Interferon gamma ELISpot of vaccine or Si-cell experienced or naïve peritoneal T cells stimulated with ovalbumin for 24 hours ex vivo (n=6 biological replicates, p=0.003 unpaired, two-tailed t tests; centres 41, 126, 188, and 37; SEM error bars). c) Antigen specificity was also evaluated in FVB mice (n=8/group) challenged with BR5-*Akt*-Luc2 cells 21 days following IP injection with vaccine cells or no antigen control mesoporous silica nanoparticles (MSN-PEI) or leukocytes (with PEI), or oxidized cell lysate, all containing CpG and MPL (n=8/group; Holm-Sidak multiple comparison). Therapeutic benefit of IP verses SC vaccination was also evaluated (n=4/SC group). Tumour burden are presented graphically and as IVIS image for each study. Individual animal curves in SI. *p<0.05; **p<0.01; ****p<0.0001

Fig.4 l.
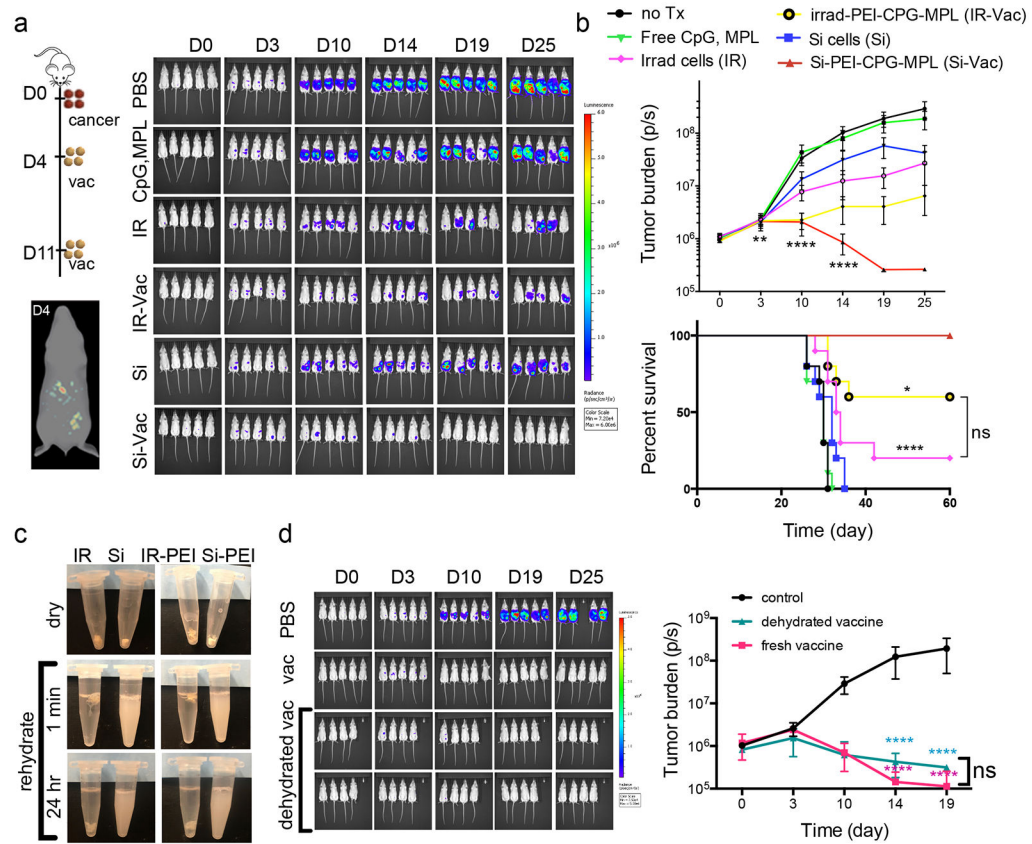
Therapeutic vaccination clears pre-existing tumours. a) Diagram of treatment schedule and tumour burden (IVIS 2D and 3D images) in FVB mice IP injected with BR5-*Akt*-Luc2 tumour cells followed by treatment with free adjuvant (free) or vaccination with silicified (Si) or irradiated (IR) cancer cells, with and without adjuvant. b) Tumour burden (photons/sec; p=0.0012 and 0.0017 for no Tx vs Si-Vac and IR-Vac, respectively; Holm-Sidak multiple comparisons) and Kaplan-Meier survival curves (n=10/group; p=0.03 for Si-Vac vs IR-Vac; Log-rank Mantel-Cox). c) Photographs of IR or Si (+/− PEI) cancer cells following dehydration (dry) and suspension in PBS (rehydrate). d) Clearance of pre-existing bioluminescent tumours in FVB mice receiving dehydrated vaccine IP on Days 4 and 11 compared to no treatment (control) or fresh (non-dehydrated) vaccine (n=4-8/group; Holm-Sidak multiple comparisons). Individual animal curves in SI. *p<0.05, **p<0.01, ****p<0.0001
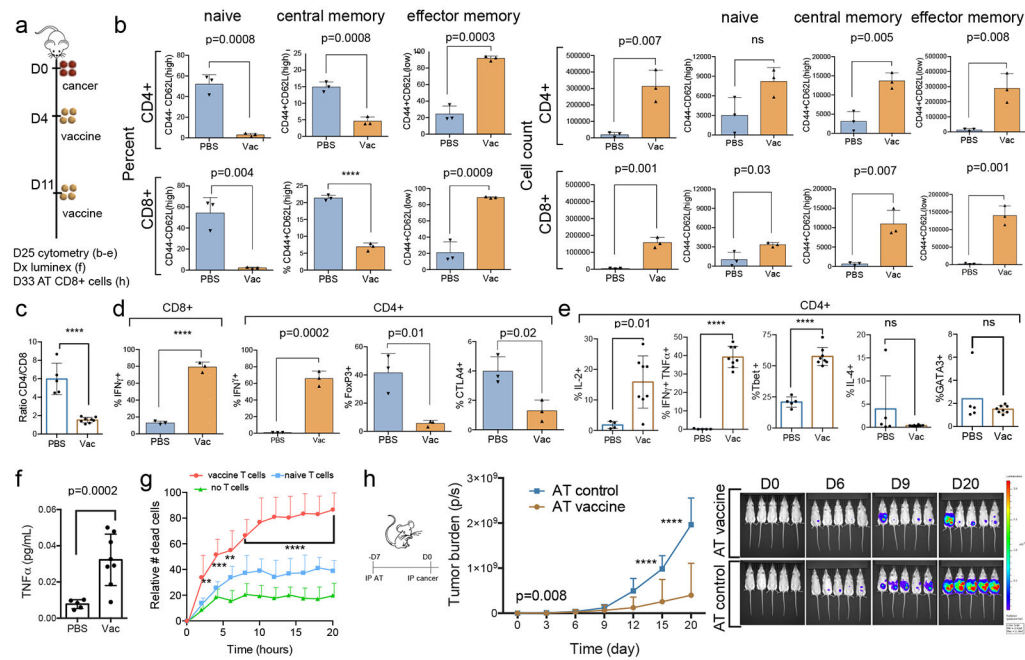
Fig.5 |.

Therapeutic benefit of vaccination is associated with significant changes in tumour-associated lymphocytes and cytokines. a-c) Flow cytometry was used to define changes in peritoneal T cell type and activation status following vaccination. Female FVB mice were IP injected with BR5-*Akt*-Luc2 cancer cells on Day 0, vaccinated on Days 4 and 11 with BR5-*Akt* vaccine cells (Si Vac) or vehicle PBS (no Tx), and peritoneal fluid/wash was collected for analysis on Day 25 (unpaired, two-tailed, parametric t-test and SD error bars). a) Percent and number of IP CD4+ and CD8+ T-cells with naïve (CD44-CD62L(high)), central memory (CD44+CD62L(high)), and effector memory (CD44+CD62L(low)) phenotypes (n=3/group; percent change centres CD4: naïve 52, 3, central memory 15, 5, effector memory 24, 92, CD8: naïve 54, 2, central memory 21, 7, effector memory 21, 89; cell count centres CD4: 19411, 313142, naïve 3017, 8194, central memory 3114, 13680, effector memory 13124, 289001, CD8: 3566, 157313, naïve 1022, 3339, central memory 637, 10957, effector memory 1886, 139802). b) Ratio of peritoneal CD4/CD8 cells (n=5-8, centres 6, 1.5). c) Percent of CD4+ and CD8+ cells expressing activation markers (n=3/group; IFNγ centres CD8 13, 79; CD4 0.7, 66), regulatory T-cell markers FoxP3 (n=3/group; centres 42, 6) and CTLA4 (n=3/group; centres 4, 1), Th1 surface markers (n=4-8/group; centres IL-2 2,16; IFNγ/TNFα 0.1, 39; and IL-4 4, 0.4), and transcription markers (n=5-8/group; centres Tbet 21, 58, GATA3 2.4, 1.5). d) Luminex cytokine analysis of ascites TNFα (n=8/group, centres 0.01, 0.03) e) Cell death (YOYO3+) in co-cultures containing peritoneal CD8+ T cells from naive (untreated) or vaccinated (Day 57) mice imaged for 20 hours using the IncuCyte Live Cell Imaging System (n=6; p=0.005, 0.0003, and 0.003 at 2, 4 and 6 hrs). f) The existence of local memory T cells was evaluated by adoptive transfer (AT) of CD8-enriched peritoneal cells from vaccinated mice to naïve mice, with IP tumour challenge 24 hours post vaccination with BR5-Akt-Luc2 cells (n=10/group; Holm-Sidak multiple comparisons; individual animal curves in SI). *p<0.05, **p<0.01, ***p<0.001, ****p<0.0001
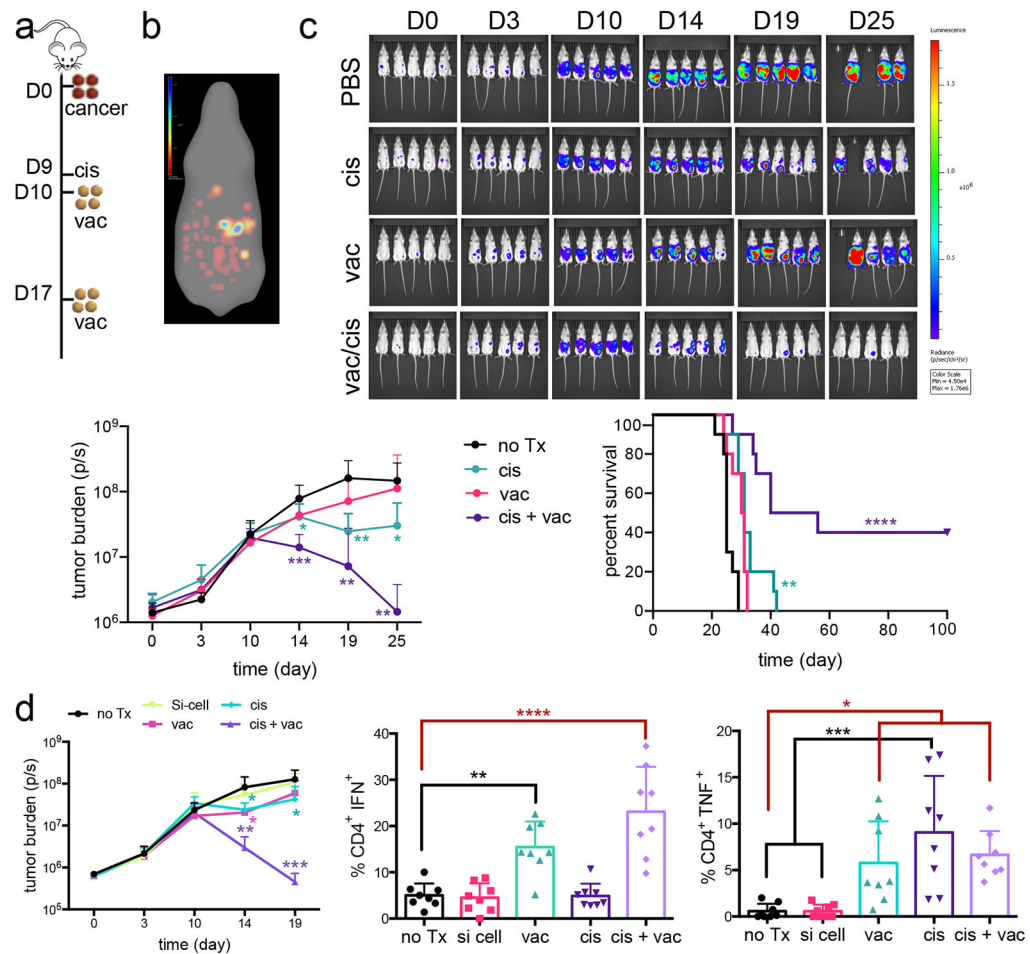
Fig.6 |.

Combination cisplatin and vaccine therapy clears established peritoneal tumours and enhances survival in mice. a) Timeline plus tumour burden (no Tx vs cis p=0.04, 0.006, and 0.013; no Tx vs cis+vac p=0.0005, 0.003, and 0.002; for Days 14, 19 and 25, respectively; Holm-Sidak multiple comparisons) and Kaplan-Meier survival curves (no Tx vs cis p=0.005; Log-rank Mantel-Cox) of BR5-*Akt*-Luc2 tumour-bearing FVB mice treated IP with cisplatin (cis, Day 9) and/or vaccine (vac; Days 9 and 17) (n=10/group). b) Tumour burden from replicate study (no Tx vs cis p=0.02 for Days 14 and 19; no Tx vs vac p=0.016 Day 14, no Tx vs cis+vac p=0.003 and 0.0006 for Days 14 and 19). Flow cytometry analysis (Day 20) of peritoneal T cell activation status [n=6-8 biological replicates; unpaired, two-tailed, parametric t-test and SD error bars IFNγ/: no Tx vs vac p=0.002; TNFα: no Tx vs vac (p=0.049) and cis+vac (p=0.015), and cis vs no Tx or si cell (each p=0.0004); centres IFNγ 5, 5, 15, 5, 23, TNFα 0.6, 0.6, 5.8, 9.1, 6.6]. Individual animal curves in SI. *p<0.05, **p<0.01, ***p<0.001, ****p<0.0001
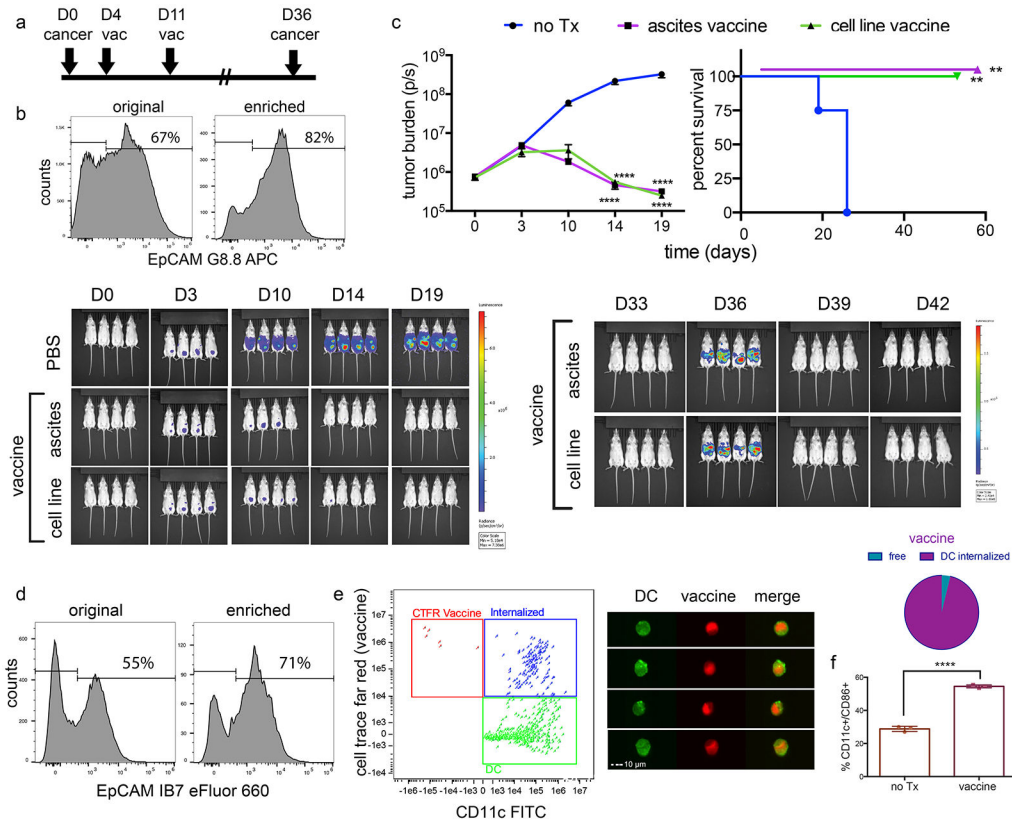
Fig.7 |.

Effective vaccine can be developed from ascites. a) Treatment schedule and timeline. b)
Flow cytometry analysis of mouse ascites cancer cell enrichment using filtration capture.
c) Tumour burden (Holm-Sidak multiple comparison; individual animal curves in SI),
Kaplan-Meier survival curve (Log-rank Mantel-Cox), and corresponding IVIS Spectrum
bioluminescent images for mice IP vaccinated on Days 4 and 11 with vaccine prepared
using the BR5-*Akt* cell line (BR5 vac) or ascites tumour cells (n=4/group; curve comparison
p= 0.0009, no Tx vs BR5 p=0.01, vs ascites p=0.01). d) To test immunological memory,
vaccinated mice were re-challenged with BR5-Akt-Luc2 tumour cells on Day 36. e) Flow
cytometry analysis of cancer cell enrichment from a human ascites sample. f) Imaging
cytometry analysis of Si vaccine cell uptake by human ascites DC. g) Human DC activation
by human Si vaccine cells based on CD86 expression (n=3 biological replicates, unpaired,
two-tailed, parametric t-test and SD error bars, centres 29, 55). **p<0.01, ****p<0.0001